“Organic Dye Functionalized CuO Nanoparticles: synthesis, characterization and applications in solar cells”

Islamabad

A dissertation submitted to the Department of Chemistry, Quaid-i-Azam University, Islamabad, in partial fulfillment of the requirements for the degree of

Master of Philosophy

in

Physical Chemistry

by

ARIF ULLAH KHAN

Department of Chemistry

Quaid-i-Azam University

Islamabad

2015

IN THE NAME OF ALLAH

THE SUPREMELY MERCIFUL AND BENEFICENT

Dedicated

To

My Mother

A strong and gentle soul who taught me to trust in

Allah, believe in hard work and that so much could be done with little

My Father

For earning an honest living for us and for supporting and encouraging me to believe in myself

DECLARATION

This is to certify that this dissertation entitled as "**Organic Dye Functionalized Nanoparticles, its synthesis, characterization and applications in solar cells"** submitted by ***Arif Ullah Khan*** is accepted in its present form by the Department of Chemistry, Quaid-i-Azam University, Islamabad, Pakistan, as satisfying the dissertation requirements for the degree of ***Master of Philosophy***in ***Physical Chemistry*****.**

Supervisor: _____

Dr. Syed Mujtabah Shah

Department of Chemistry

Quaid-i-Azam University

Islamabad.

Head of Section:

_____

Prof. Dr.Muhammad Siddiq

Department of Chemistry

Quaid-i-AzamUniversity

Islamabad.

External Examiner:

_____

_____

Chairman:

_____

Prof. Dr. Amin Badshah

Department of Chemistry

Quaid-i-AzamUniversity

Islamabad.

ACKNOWLEDGEMENT

It is indeed a great honor for me that I have completed this research work for M.Phil (Chemistry). Although it was a difficult task but it was due to the special investiture of Almighty Allah, Who blessed and enabled me to complete this work.

I am greatfull to the personalities who generously contributed their time and effort to help me make this research work as accurate & as useful as possible.

I would particularly like to express my deepest thanks to my supervisor **Dr. Syed Mujtaba Shah**, Assistant Professor, Department of Chemistry, Quaid-I-Azam University, Islamabd. I highly valued his support of my work in department of Chemistry who have encouraged me & provided valuable information in this research work & other teaching work.

I would also like to thanks **Prof. Dr. Amin Badshah** Chairman Department of Chemistry Quaid-I-Azam University Islamabad for his support and guidance. I offer my deep and sincere thanks to all the teacher of Chemistry Quaid-I-Azam University Islamabad.

My special thanks to Head of Physical Section, Department of Chemistry, Quaid-I-Azam University, Islamabad, **Prof. Dr. Muhammad Siddiq** for his keen interest, precious attention, and continuous encouragement. I am grateful to for his very kind behavior.

I acknowledge with gratitude the otmost support of my seniors and lab fellows, **Fakhre Alam**, **Zubair Hassan and Banafsha Habib**, without their support I was unable to complete my M.Phil work.

Special thanks to all staff members of this department for their help and cooperation throughout my research work. I would like to express my sincere appreciation and thanks to all my class Fellows and friends especially **Hanif Subhan, Shakir Ullah, Zaffar Iqbal Abdul Haleem and Muhammad Farooq.**

I particularly want to acknowledge the tremendously helpful, supportive contribution of my family, my respective Parents, my elder brothers **Shah Hussian** (Asst: Prof in Physics) and **Muhammad Shoaib Khan** and my sweet sisters, who gave time and good enviro nment for the completion of this research work.

ARIF ULLAH KHAN

CONTENTS

LIST OF FIGURES

ABSTRACT

In this study copper oxide nanoparticles were synthesized successfully by sol-gel method using anhydrous copper chloride ($CuCl_2$) as a precursor and sodium hydroxide (NaOH) as a strong stabilizing agent. Photosensitization of CuO nanoparticles was carried out with brilliant blue red (BBR) dye. The synthesized materials were characterized by UV-Visible spectroscopy, fluorescence spectroscopy, X-ray powder diffraction, infrared spectroscopy, scanning electron microscopy and energy dispersive spectroscopy. Dye sensitized solar cell was fabricated using the synthesized material as a photo-active blend and efficiency of the fabricated device was calculated at different dye concentrations.

CHAPTER-01

INTRODUCTION

From the last few decades, energy crisis has become a burning issue which leads to increasing demand of solar power generation across the globe[1, 2]. Being an ultimate and inexhaustible energy source, sun deliver a large amount of energy to the earth surface in the form of electromagnetic radiation, released from various types of nuclear reactions[3]. Surface power density of the solar radiation outside the atmosphere is called solar constant and its numerical value is 1.37KW/m^2[4]. However on the surface of the earth this value is 174.7W/m^2, because 30% of this flux is scattered and about 19% is absorbed by various components of atmosphere like ozone, carbon dioxide, oxygen and water vapors. In other words earth surface receive solar energy at the rate of 120 pet watts per day which is sufficient for the whole world up to 20 years. According to one of the estimate earth receive 1.7×10^{22} joules amount of energy in 1.5 days, which is equal to the amount of energy obtained from 3 trillion barrels of oil.

1.1. Solar cell

Solar cell is a photovoltaic device which directly converts solar energy into electrical energy without being converting it to other form of energy like thermal, chemical etc. The conversion of light energy into current or electromotive force is preferred over other energy harvesting processes because it does not require other form of energy for its maintained.

1.1.1. Operation principle

The basic operation principle of solar cell is the photovoltaic effect [5, 6]. Photovoltaic effect was demonstrated by nineteen year old Edmond Becquerel in 1839 while working in his father's laboratory[7]. Photovoltaic effect is actually the conversion of photon energy into electrical energy[8]. During experiment he stroked silver coated platinum electrode dipped in acidic solution with sunlight. After striking the electrode with sunlight the flow of current was started in the external circuit[9]. This experiment stimulated Becquerel and his co-workers to develop such a powerful system that utilize large amount of sunlight

energy for generating electric current, but every time they failed. Later on, it was realized that this effort is possible by using doped semiconductor having p-n junction.

1.1.2. A typical solar cell

To design a photovoltaic cell n- and p-types semiconductors are sandwiched together which form a p-n junction. This junction lies at their interface and allow the electrons flow in forward direction but not in reverse biased. Although both types of semiconductors are electrically neutral, but when a p-n junction is formed electrons from n-type diffuse to p-type creating negative charge on electron deficient material and leaving positive charge on opposite side near the junction. This charge separation leads formation of electric field which acts like a diode, pushing the electrons from p type to n type material and inhibit their flow in the reverse direction.

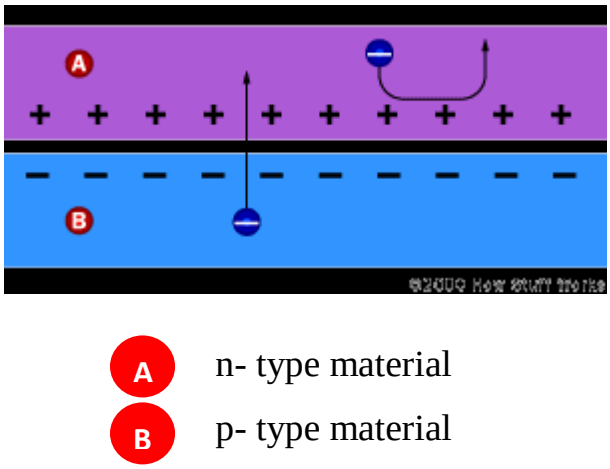

Figure 1.1 *Showing p-n Junction*

Under the influence of electric field, electron not only cross the junction but also move to the surface of the material and hence become available for producing potential difference in the external circuit. The electrons are excited from valence band to the conduction band when they absorb light in the depletion region. These free electrons are either pulled to n-type region by electric field or get excited to the conduction band on either side of the junction. From here, the electrons reach the depletion region through diffusion process and finally pulled to n type region under the influence of electric field. By applying external load to photovoltaic cell electron start flowing through the external circuit and reach p type where they recombine with holes. Moreover the light generated current is independent of the applied voltage except in amorphous silicon and some thin film solar cells [10, 11].

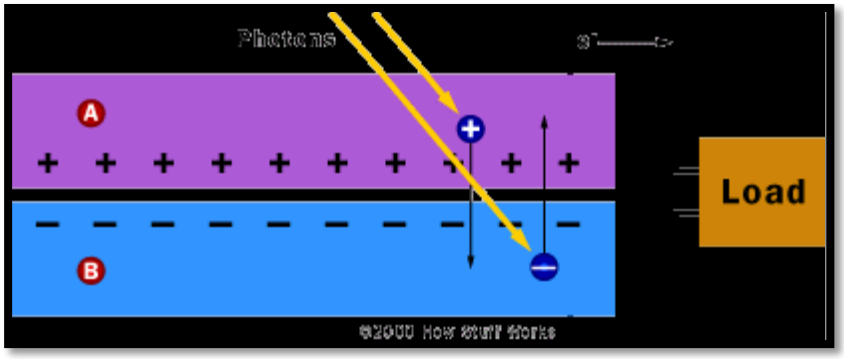

Figure 1.2 *Operation of a solar cell*

1.2. Historical developments

The history of solar cell started from 1839 when nineteen years old Edmund Becquerel observed the photovoltaic effectfor the first time. However in solid materials like selenium the same effect was observed by two British scientists Grylls Adams and Richard in 1870s. In the 1880s, Charles Fritt designed the first photovoltaic device using selenium, but its efficiency was very low and about 1% -2% of light was converted to electricity. Till the first half of twentieth century it was used as photometric device for measuring light intensity. In 1920s and 1930s quantum mechanics provided the theoretical base for photovoltaic cell.

The direction of development of the solar cell was turned when Czochralski produced highly purified monocrystalline silicon. In 1954s, two Bell labs scientists Calvin Fuller and Gerald Pearson constructed a photovoltaic cell using monocrystalline silicon[12]. The efficiency of this cell was about 4% and later on it was improved up to 11%. Many attempts were made to commercialize these types of solar cell for power generation, but each time unexpected results came from different parts of the world. In 1958s, the united state department for space used a solar cell of about one-watt power to run the radio of space satellite. The cells run the radio in satellite so well that scientists became interested for their development. According to the Yole department in 2007, silicon based solar cell will dominate all other types of solar cells in the world[13]. So far, the element silicon is the best choice for terrestrial photovoltaic cell[14-16] owing to its more abundance(second most abundant) and ideal band gap for harvesting solar spectrum[17][18].

Due to the recent advancement in this active research domain, such solar panels have been developed which convert one kilowatt of solar energy, striking the panel of one square meter, into hundred kilowatt of electricity. In the United State 3.2 million houses are powered by solar cells. Besides this, in 2014, 53% of all new electrical generation installed has come from solar energy. The world largest floating solar power plant is located in Japan having total capacity of 1.7 megawatts. The solar panel companies are determined to install 60 MV of floating solar by the end of March 2015.

1.3. Solar cells generations

1.3.1. First generation

First generation solar cells are usually made of phosphorous and boron doped silicon. These cells are suitable for those regions where light intensity is low and limited space is available [19]. Compared to other silicon based solar cells the conversion efficiency of monocrystalline silicon based solar cell is high, about 24% at laboratory level and 17% at commercial scale[20, 21]. But, these cells are very expensive as highly purified silicon is required for its manufacturing. Another issue with monocrystalline solar cell is decrease in their efficiency with increase of temperature. So the panel should be installed in such a manner that the air circulate through the panels. Besides this, their efficiency also decreases with the passage of time and after 50 years they completely lose their efficiency. Despite all these disadvantages they are the most dominant solar cells at commercial level and up to 2007, 89.7% products are accounted for commercial production.

1.3.1.1. Production of monocrystalline silicon

Silicon is the most important and second most abundant element in the periodic table. Naturally, it exists in various forms like silica or sand, rock crystal, quartz and quartzite which constitute 25.7% of the earth crust. Among its various forms, quartzite is commonly used for the production of monocrystalline silicon. The various steps for its purification are described below.

- Initially, quartzite is treated with carbon in the form of wood, coke, or coal at 2000℃ to form metallurgical grade silicon(98% pure)[22].
- The silicon produced contains impurities, which is further purified by treating with concentrated hydrochloric acid at 1200 ℃ to form trichlorosilane. Further, the impurities present in the liquid trichlorosilane are removed by fractional distillation.

- The purified liquid is reacted with hydrogen gas at high temperature to form electronic grade silicon, which is also called polycrystalline silicon or polysilicon by well-known Siemens` process.
- Finally, polysilicon crystals are converted to monocrystalline silicon by Czochralski process, in the honor of a polish chemist Jan Czochralski who first introduced this technique, in 1918. A major disadvantage associated with this process is the slow growth rate about 0.5 inche per hour leading to more energy consumption that's why their wafers are very expensive. Chemical equations of the different steps are given below.

$$SiO_2 + 2C \xrightarrow[2000℃]{\text{Heat}} Si + 2CO \quad \text{(MGS)}$$

$$Si + 3HCl \xrightarrow[1200℃]{\text{Heat}} SiHCl_3 + H_2$$

$$2SiHCl + 2H_2 \xrightarrow[1100℃]{\text{Heat}} 2Si + 6HCl \quad \text{(EGS)}$$

1.3.1.2. The Shockley-Queisser limit

According to William Shockley and Hans Queisser in 1961, efficiency of a single junction solar cell with a band gap of 1.28 eV cannot exceeded than a theoretical limit of 30%, which is called detailed balance limit or Shockley-Queisser limit[17]. Later on in 1977, Robert Ross and Ta-Lee Hsiao generalized this concept for all types of photovoltaic devices[23]. The principle of detailed balance is based upon the second law of thermodynamics. Two kinds of factors, extrinsic and intrinsic are involved in efficiency loss of a photovoltaic device. Extrinsic factors like reflection and series resistance can be removed by fabrication the device in a proper manner. However intrinsic losses cannot be removed by any type of method and this is the main reason that efficiency of a photovoltaic device is limited up to 30%.

Mathematically the efficiency of a solar cell having a single p-n junction is given below,

$$\eta\,(X_c, X_g, t_s, \text{f}) = \text{m}\,(X_c, X_g, \text{f})\ \upsilon\ (X_c, X_g, \text{f})\ \mu\ (X_g) t_s$$

Where

η (X_c, X_g , t_s, f) is the total efficiency

μ (X_g) is the ultimate efficiency

m (X_c, X_g , f) is the impedance matching factor

υ (X_c, X_g , f) is the ratio of output voltage and band gap

t_s is the probability of a photon to create electron-hole pair

1.3.1.2.1. The ultimate efficiency

The ultimate efficiency represents the loss of solar energy due to band gap of the photovoltaic device. As all types of photons are unable to excite the electrons, photons having energy equal or greater than band gap are absorb and cause excitation of the electrons. On the bases of this concept, Shockley and Queisser derived the ultimate efficiency equation. Consider a p-n junction having temperature T_c=0 which is surrounded by a black body with temperature T_s, hence ultimate efficiency can be calculated as,

$$\mu (X_g) = \frac{photon\ energy\ generated}{input\ power} = \frac{Q_s h\upsilon_g}{\mathbf{P_s}}$$

Where Q_s represents the numbers of incident photons per unit area per unit time.

1.3.1.2.2. View factor of the sun

Let suppose A_p and A_s are the surface areas of the photovoltaic device and the sun respectively. Then the area of the device projected to the solar radiation is $A_p \cos\theta$, thus the view factor from the solar cell is $\frac{A_p \cos\theta}{4\pi L^2}$, where L represents the distance of the earth from the sun. So the incident power striking the surface of the solar cell is given below

$$P_{inc}=P_s(\frac{A_p \cos\theta}{4\pi L^2})A_s=P_s(\frac{A_p \cos\theta}{4\pi L^2})\,4\pi R^2$$

$$= P_s A_p\,(\frac{\pi R^2}{L^2})\frac{\cos\theta}{\pi} = P_s A_p \omega_s \frac{\cos\theta}{\pi} = P_s A_p f_\omega$$

Where R represent radius of the sun, ω_s is the solid angle and f_ω is called geometrical factor, which can be written in the following mathematical form

$$f_\omega = (\frac{\cos\theta}{\pi})\,\omega_s$$

From these parameters we can calculate the rate at which electron-hole pairs are generated

$$F_s = Q_s A_p t_s f_\omega$$

1.3.1.2.3. Recombination

When a solar cell is connected to the external load then all the excited electron-hole pairs are not passes through the external circuit, because most of them lose their energy by recombination. Inside a photovoltaic device usually two types of recombination process takes place, radiative and non-radiative recombination. In radiative recombination electron and hole react with each other to produce a photon which is the inverse of photon absorption.

$$e + h \rightarrow \gamma$$

The process of radiative recombination or annihilation increases with the concentration of electron-hole pairs. Sometime the photon released during the annihilation process cause regeneration of the electron-hole pair.

Non radiative recombination may be either auger recombination or impurity recombination. In auger process the released energy during recombination is given to a hole and an electron as kinetic energy. The newly excited electron-hole pair loses their energy by effective collision with the atoms of the lattice within the semiconductor. It is a reverse process of impact ionization where atom's electrons are ejected by high energetic electron.

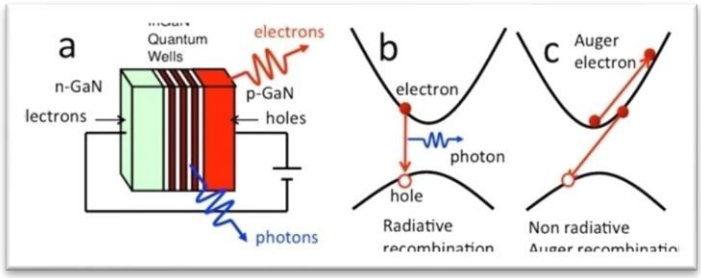

Figure 1.3 *Radiative and non-radiative Recombination*

In 1952, Shockley-Read-Hall proposed a model to explain the recombination via impurities[24, 25]. According to this model, due to the presence of impurities there exist some energy levels between the valence and conduction bands which are known as defect levels or trap levels. Electrons can relax from the conduction band to the valence band through these defect levels, cause annihilation of the hole in the valence band, while releasing energy in the form of phonons. Moreover the former one is intrinsic which cannot be

eliminated theoretically, while the later one can be removed by various fabrication techniques.

1.3.1.2.4. Impedance matching factor

Practically in a solar cell, the values of open circuit voltage and short circuit current cannot be obtained simultaneously. Rather than, maximum values of current and voltage is achieved at the condition when optimized load is applied, however there values are much smaller than V_{opn} and I_{sct}. Before going to explain the actual efficiency, first we define the nominal efficiency which is the ratio of the product of V_{opn} andI_{sct} to the incident power, when the external load is not yet connected to the solar cell.

$$\eta \text{ (nominal)} = \frac{I_{sct}V_{opn}}{P_{in}}$$

However the impedance matching factor can be define as

$$\text{m} = \frac{I_{max}V_{max}}{I_{sct}V_{opn}}$$

So the actual or practical efficiency is the product of impedance matching factor and nominal efficiency which can be written as

$$\eta \text{ (practical)} = \left(\frac{I_{max}V_{max}}{I_{sct}V_{opn}} \right) \left(\frac{I_{sct}V_{opn}}{P_{in}} \right)$$

$$= \frac{I_{max}V_{max}}{P_{in}}$$

$$\eta \text{ (practical)} = \frac{P_{max}}{P_{in}}$$

1.3.2. Second generation

Second generation solar cells, also known as thin film solar cells because a very thin layer of silicon is deposited on different materials at temperature around 200℃. A major advantage related to this type of solar cells is that it requires a very small amount of silicon compared to classical crystalline silicon based solar cell which reduces their costs. Second generation solar cells can be categorized into three types.

1.3.2.1. Amorphous silicon

Amorphous silicon were first of all reported by R. Chittick in 1965[26]. Later on, W.E. Spear and LeComber at Dundee University, demonstrated that phosphorous and boron doped amorphous silicon had semiconducting properties[27]. This discovery leads the scientists to use amorphous silicon in fabrication of solar cells, because initially it was thought that this form of silicon could not be doped with any type of impurities. The amorphous silicon used in solar cell or other electronic devices is an alloy of silicon and hydrogen therefore it is also known as hydrogenated amorphous silicon. Hydrogenated amorphous silicon have a high absorption coefficient, a layer of one micrometer thickness can absorb about 90% light in the visible range of the solar spectrum. As the semiconductor is deposited at low temperature of about 200℃, therefore a variety of substrates like polymer foil, metal and glass can be used for the deposition of amorphous silicon.

The first hydrogenated amorphous silicon based solar cell was fabricated by Carlson and Wronski in 1976[28]. The efficiency of that cell was about 2.4%, but later on this efficiency was improved up to 15%. Now-a-days, out of the total module production in the world, 6% photovoltaic modules are based upon the amorphous silicon.

1.3.2.2. Copper indium gallium diselenide (CIGS)

This material was first of all introduced by Hahn in 1953. Late on, in 1974 it was proposed that it can acts as photovoltaic material. After 10 years, B Corp reported a thin film made up of CIGS having efficiency more than 10%. The band gap of CIGS ranges from 1.04eV to 1.7eV. The structure of CIGS consists of the following components.

1) Substrate like polyimide, foil, ceramic and glass
2) Molybdenum of 0.5μm thickness as back contact
3) Thin film of CIGS as absorption layer (p-type)
4) Cadmium sulphide deposited as buffer layer (n-type)
5) ZnO and aluminum doped ZnO (AZO) as transparent front contact

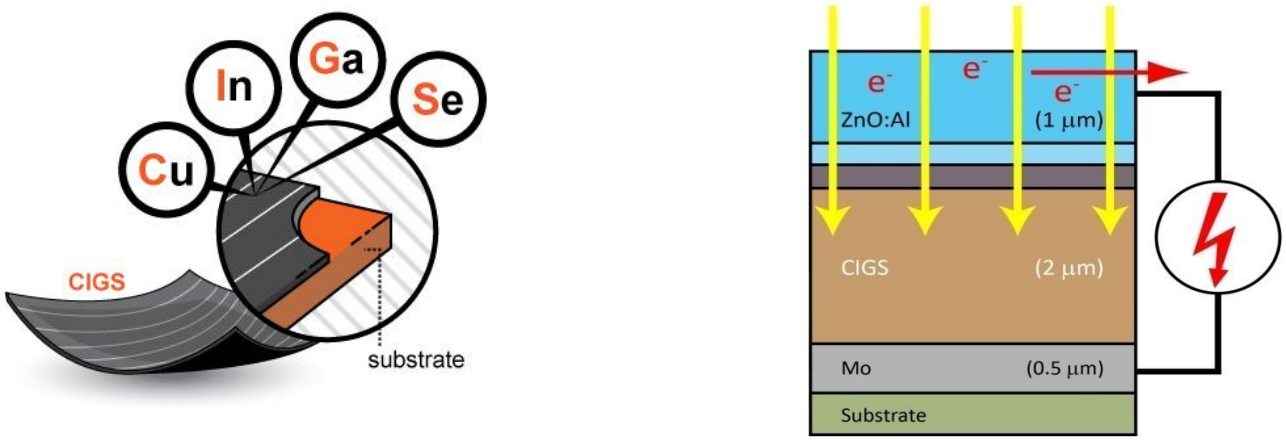

Figure 1.4 *CIGS Structure and working principle*

1.3.2.3. CdTe based solar cells

Cadmium telluride is an II-VI type semiconductor which is considered one of the best materials for low cost solar cells. The band gap of CdTe is 1.5eV, which is an ideal value to the sun spectrum for photovoltaic conversion. The expected theoretical efficiency CdTe based solar cell is about 28%[29]. However the actual efficiency achieved at the laboratory level is 15.8% [30]. This type of solar cell consists of the following main parts.

1) Glass as transparent substrate
2) Transparent conductive oxide of 1μm thickness (TCO)
3) CdS window layer of 0.07 μm thickness
4) Absorbing layer of CdTe
5) Back contact

1.3.3. Third generation

Although it consists of many types of solar cells but the most notable among them is the dye sensitized solar cell abbreviated as (DSSCs), which is the prime focus of the current study.

1.3.3.1. Dye-sensitized solar cells(DSSCs)

The DSSCs represents an attractive and smart choice due to its low cost of the material[31]. These can be differentiated from other types of solar cells due to its capability of handling exciton and light absorption by different parts[32, 33]. The development of dye sensitized solar cells started, when zinc oxide electrode was sensitized by chlorophyll pigments in 1972. However, the efficiency of such types of devices was very low and only

1% of the solar radiation was absorbed by a monolayer of pigment molecules. Later on, in 1991, Michael Gratzel and Brian O'Regan introduced titanium oxide nanoparticles and demonstrated that these particles provide a large surface area for dye encoring. This concept increased the efficiency of dye sensitized solar cells up to 7% and today their efficiency is about 11.2%, which allowed them to compete with all other types of solar cells[34].

1.3.3.1.1. Structure and constituents of DSSCs

1.3.3.1.2. Working electrode (TiO_2)

Titanium oxide (TiO_2) exists in three different crystalline forms namely brookite, anatase and rutile. Although both anatase and rutile can be used in DSSCs but the former is preferred due to its wide band gap (3.2eV) and excellent photo-catalytic properties. The DSSCs using TiO_2 as working have highest efficiency compared to other semiconductor oxide including ZnO and SnO_2. The effect of titanium oxide nanoparticles size on the efficiency of dye sensitized solar cells was first studied by Chou and his coworkers. The efficiency of DSSCs increases with increase of particle size and become tripled when the nanoparticles size is increased from 10 nm to 22 nm[35].

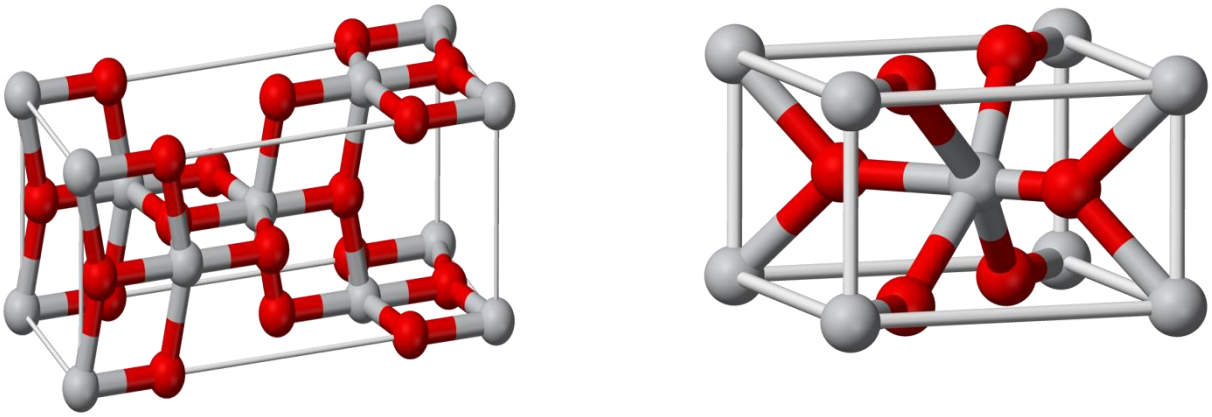

Figure 1.5 *Unit cell for: (1) anatase TiO_2 and (2) rutileTiO_2*

.

1.3.3.1.3. Sensitizer

The main problem of DSSCs is the wide band gap of titanium oxide nanoparticles which results in the shift of light absorption to ultraviolet region instead of visible region. Furthermore, only 2% light of the solar spectrum can be absorbed in the ultraviolet region[36]. To solve this problem, various types of organic dyes and transition

metal complexes chemically adsorbed on TiO_2 nanoparticles. To use a dye as sensitizer it should full fill the following requirements.

1) The absorption spectrum of the dye should be broad, extending from 4000Å to 10^6Å.
2) There will be minimum chances of the excited dye molecules to deactivate through the emission of photon or phonon.
3) The dye should be adsorbed chemically at the surface of the working electrode and there will be a strong interaction between the conduction band of the electrode and excited state of the dye.
4) For the prolonged working of the DSSCs the stability of the dye in oxidized, excited as well as in the ground state is very important.
5) For an effective electron injection the dye should have higher value of reduction potential than the conduction band of the material.
6) For the rapid regeneration, the dye should have lower value of oxidation potential than the redox couple.

1.3.3.1.4. Electrolyte solution

Electrolytic solution plays a key role in dye sensitized solar cells because it allows internal conductivity of the ions[37]. Nowadays, for high efficient DSSCs, electrolytic solutions based on volatile organic solvents (VOS) are commonly used. Some important VOS are methoxypropionitrile, methoxyacetonitrile, propionitrile and acetonitrile, which are selected for their high value of dielectric constant, ionic conductivity and electrolytes dissolution ability. Their commercial scale applications in DSSCs are limited by poor long term stability. Besides this, polymer electrolytes, inorganic p type semiconductors and ionic liquid electrolytes are also used in DSSCs. The properties like good ionic conductivity, non-inflammability, chemical stability and non-volatility make the low temperature ionic liquid to compete with volatile organic solvents. However the viscosity of RTIL is 100 times greater than volatile organic solvents, which reduces the photo generated current by increasing the internal resistance.

In solid-state dye sensitized solar cells the most commonly used material for holes transportation is the p type semiconductor. Not all types of p-type semiconductors can be use in a DSSCs, it must full fill the following conditions.

1) The ground state of the sensitizer must be located below the valance band of the p-type semiconductor, so that the holes are transfer to it and the dye will be regenerated.

2) The p-type semiconductors are deposited in such a manner, to avoid degradation of the dye.
3) The efficiency of the p-type semiconductor to inject electron is same as that of the dye.

There are some inorganic p-type semiconductors which usually fulfill all the above requirements, but as they are deposited at high temperature which usually degrade the dye, so they are not suitable to use in dye sensitized solar cells. The examples of such materials are SiC and GaN. However copper based halides and cyanides (CuI, CuBr, CuSCN) not only satisfy these requirements but also deposited at low temperature without any damage to the dye[38].

1.3.3.1.5. Redox couple (I^-/I_3-)

Iodide salts are commonly used for ionic conductivity in DSSCs. Although, it enhances the efficiency of solar cell but it also have some adverse effects on the performance of DSSCs. Firstly, extra voltage of 0.5-0.6eV is required for dye regeneration because the positive redox potential of (I^-/I_3-) is lower than ruthenium based dyes leading to consequent decrease in efficiency of the cell. Secondly, the trioxide species of iodine couple absorb light in the visible region of solar spectrum. Other types of redox couples such as coordination complexes, (Co^+/Co^{2+}), (Co^{2+}/Co^{3+}), SCN-/(SCN)3 and SeCN-/(SeCN) 3- have also been explored but their efficiency is lower than (I^-/I_3-)[39].

1.3.3.1.6. Counter electrode

It is one of the key components of DSSCs used for dye regeneration after its oxidation by absorbing light[40]. Platinum based electrode is the most commonly used counter electrode which is a thin film of platinum deposited on transparent conductor oxide (TCO). Platinum counter electrode is one of the best choices for the reduction of redox couple due to its high conductivity, stability and good catalytic activity. Instead of platinum other types of materials like metals, carbon black, graphite, carbon nanotubes and activated carbon can also be used for the counter electrodes. Metals like nickel and steel cannot be used as counter electrode due to corrosive nature of the iodide redox couple. To use such materials they should be deposited with anti-corrosion substances like fluorine doped SnO_2 and carbon.

1.3.3.1.7. Operation mechanism

When light in the visible region of the solar spectrum strike the DSSCs, electrons from the highest occupied molecular orbital are excited to lowest unoccupied molecular orbital of the dye molecules. After that, these excited electrons are injected from the LUMO of the dye into conduction band of the nanoparticles. The charge carriers or electrons are localized on dye molecules because of the poor intermolecular forces among the molecules and therefore its transformation occur from one molecule to other following a proper channel. These electrons are migrated to transparent conductive oxide (TCO) on which [TiO_2] nanoparticles have already been pasted. The electrons are passed through the external circuit where they do some electric work. Finally, electrons recombine with holes, created by the redox couple in the counter electrode. Some time it may happen that electrons from the conduction band of the nanoparticles migrates to the HOMO level of the electrolyte or dye, without passing through the external circuit. Such process are known as, electrons back reactions which greatly affects the efficiency of DSSCs. Back reaction depends upon the kinetics of electron transferring from one species to other[41, 42]. The most efficient DSSCs have the following characteristics.

1) The decay rate of the excited dye should be slower than the rate of electron injection.
2) The rate of back reaction of the dye with the excited electron must be slower than the reduction of the dye by redox couple.
3) The reduction of the redox couple at the counter electrode should be very faster[43].

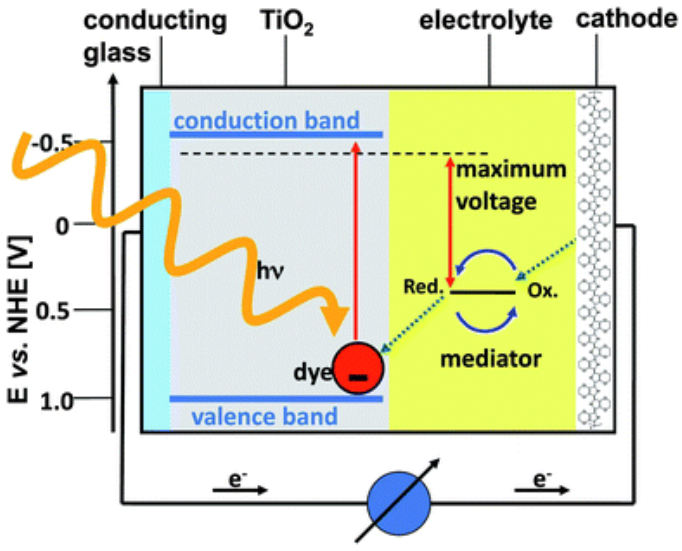

Figure 1.6 *Working principle of DSSC*

1.3.3.1.8. Nanotechnology in DSSCs

Nanotechnology is the study of the materials at the nanoscale, ranging from one nanometer to hundred nanometers[44]. In the last two decades, dramatic advances have been made in this area as different nanostructures like nanobelts, nanotubes, nanowires, nanoparticles etc. have been developed. The efficiency of DSSCs depends upon the light capturing component or antenna, which is usually an organic dye. As for the adsorption of dye, nanomaterials provides a large surface area as compare to bulk materials, so they play a key role in DSSCs. The nanoparticles provide a large specific surface area as compare to other nanomaterials, so it is the best choice for making photo anode in DSSCs[31, 45]. The charge transfer in photoelectrode composed of nanocrystalline film are hundred times slower than the nanowires electrode, which increase the chances of recombination of the excited electrons with holes in the electrolyte[46, 47]. Besides this, oxide aggregates can also be use as nanomaterials in DSSCs. These aggregates are basically micron sized spheres, which are usually synthesize by aggregation of nanoparticles[48, 49]. They not only provide support for the adsorption of dye but also cause the effective scattering of light in the visible region of sun spectrum. The efficiency of DSSCs became double, when zinc oxide aggregates are used instead of dispersed nanoparticles in the working photo-electrode. Based on size and structural properties, nanomaterials are classified into four types.

1) Nanoparticles, which provides large surface area for dye adsorption, however greater recombination chances for excited electrons with holes in the electrolyte.
2) Nanotubes and nanowires, provide a straight path for charge transportation, but have insufficient surface area for dye adsorption.
3) Core-shell structures covered by a coating layer to reduce the chances of recombination, however they are also less effective and lack of stability.
4) Oxide aggregates, which not only provide a large surface area but also scattered the visible light of the solar spectrum.

1.3.3.1.9. Core-shell nanostructures

A serious problem associated with DSSCs is the charge recombination which reduces the photogenerated current. In this process, the photo-excited electrons react with holes of the redox couple in electrolyte. This limitation affects the photogenerated current and open circuit voltage by decreasing the forward injection current and electrons concentration in the conduction band respectively[50, 51]. To remove these drawbacks, core-shell

nanostructures are used in dye sensitized solar cells. They are basically nanomaterials like nanotubes, nanowires or nanoparticles covered by a coating layer. This coating layer acts as energy barrier at the interface of electrolyte and semiconductor, which inhibit the recombination of the photoexcited electrons with holes of the redox couple. For the syntheses of core-shell nanoparticles two methods are applied.

1) First synthesize the nanoparticles and then covered the particles by a coating layer. After that they are pasted on the surface of conducting glass to use it as working photoelectrode. In such cases the coating layer is an energy barrier for the interface of nanoparticles and electrolyte and also for individual nanoparticles.
2) In the second method, the nanoparticles are pasted on the surface of the conducting glass and after that a shell coating layer is fabricated on it. In this case the coating layer is the energy barrier only for the electrolyte/nanoparticles interface.

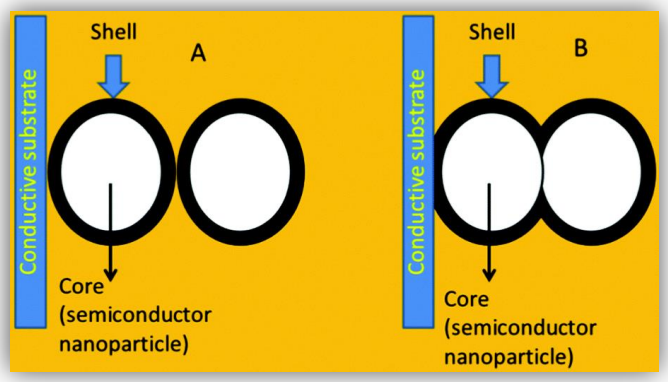

Figure 1.7 *Core Structure of Semiconducting nanoparticle*

To use materials for shell coating layer, they must have more negative conduction band potential than the core material. Experimentally it was proved that, both short circuit current and open circuit voltage increased by 37%, when various oxides like $[ZrO_2]$ and $[ZnO]$ coated $[TiO_2]$ were used instead of bare titanium oxide.

1.3.3.1. Synthesis of nanomaterials

Synthesis of nanomaterials in a way to retain its crystalline structure, size and shape play an important role in the fields of electronics, medicines, catalysis and dye sensitized solar cells. Methods for the fabrication of nanostructures and synthesis of nanoparticles are classified into two groups, discussed below.

1.3.3.6.1. Top-down method

This approach involves the creation of nanoparticles or nanostructures by the division of bulk materials. A typical top-down approach for the synthesis of nanoparticles is attrition or milling. Other techniques involve in the top-down method are aerosol spray, gas-phase condensation, atomic force manipulation and electron beam lithography. The biggest issue related with top down is the imperfection of the surface structure or crystallographic defects. For instance, lithographically made nanowires have not only the structural defects but also their surfaces are not smooth due to the presence of impurities at the surface. This effect leads to reduction in electrical conductivity and generation of large amount of heat. In spite of the above shortcomings, this technique is still widely used for the syntheses of nanomaterials.

1.3.3.6.2. Bottom-up method

This method involves the fabrication of nanoparticles from the bottom, that is, atom by atom or the gas phase condensation of the atoms or molecules. Among the different methods of the bottom-up approach: sol-gel processing, microwave synthesis, gas-phase method, hydrothermal method and combustion synthesis are the most commonly used for the fabrication of metal oxide nanoparticles. The nanoparticles fabricated by this method have negligible structural defects as compared to the particles synthesized by top-down method.

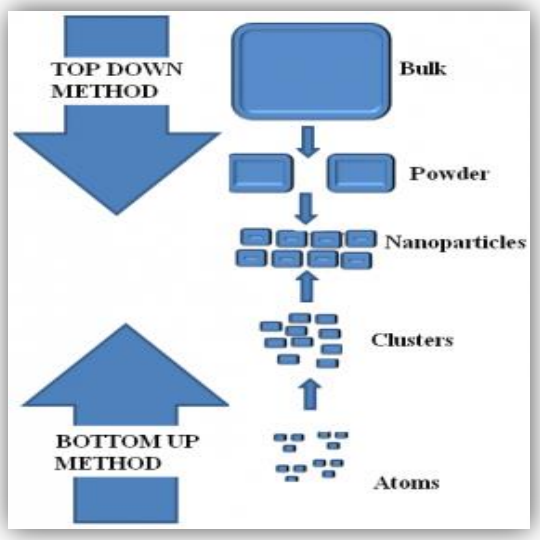

Figure 1.8 *Synthesis Routes of Nanoparticles*

1.3.3.2. Introduction to copper oxide nanoparticles

Metal oxide nanomaterials are extensively applied in the fields of catalysis, sensing, optoelectronics and solar cells owing to their unique chemical and physical properties [52]. Among the different metal oxide nanoparticles, copper oxide nanoparticles is the best choice due to its good optical and electrical properties, non-toxic nature, low cost production and natural abundance of the copper. Copper react with oxygen to form two types oxide, that are cupric oxide $[CuO]$and cuprous oxide $[Cu_2O]$. Cuprous oxide is a p-type material with direct band gap of 2 eV. It is basically II-VI type semiconductor having cubic crystal structure. On the other hand, cupric oxide is also a p-type material with indirect band gap of 1.2-1.5 eV. This type of copper oxide exists in monoclinic crystal structure. The optical absorption and catalytic activities of $[CuO]$ are equally dependent both on its size and shape[53]. As the superconductivity of cuprate based superconductors is based upon the $[CuO]$ bonding so cupric oxide also play a key role in superconductors having high critical temperature. The composites of cupric oxide with zinc oxide $[CuO - ZnO_2]$ and Tin oxide $[SnO_2]$ also have vast application in gas-sensors and humidity.

The good electrical properties and high optical absorption coefficient of cuprous oxide make it suitable for low cost photovoltaic devices. The theoretical efficiency of cuprous oxide made thin film solar cell is about 13%. However, at the interface of thin film solar cells, an oxygen- deficient or copper- rich layer is produced, which affect the efficiency of the device. The main cause of this layer is the reduction of cuprous oxide, which restricts its applications in heterojunction solar cells.

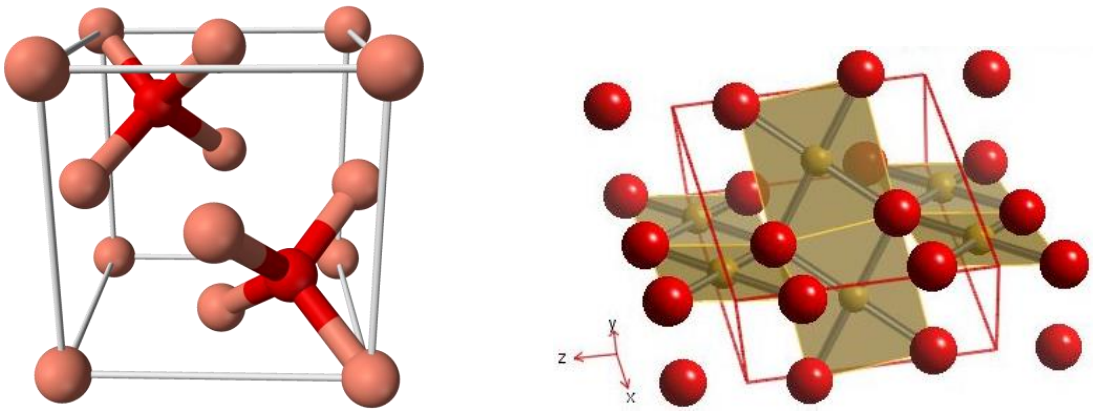

Figure 1.9 *Cuprous and cupric oxides Structures*

1.3.3.3. Coomassie brilliant blue dyes (sensitizer)

Although, there are about 40 different types of Coomassie dye but the most commonly used are Coomassie brilliant blue R-250 and Coomassie brilliant blue G-250. The absence of two methyl groups in Coomassie brilliant blue R-250 differentiates it from Coomassie brilliant blue G-250. The suffix "G" and "R" represents the greenish and reddish tint in Coomassie brilliant blue G-250 and Coomassie brilliant blue R-250 respectively, while the number "250" represents purification of both the dyes. In both the dyes the two sulphonic groups acts as anchoring groups which lead the dyes to adsorb on the surface of the material for light absorption in dye sensitized solar cells.

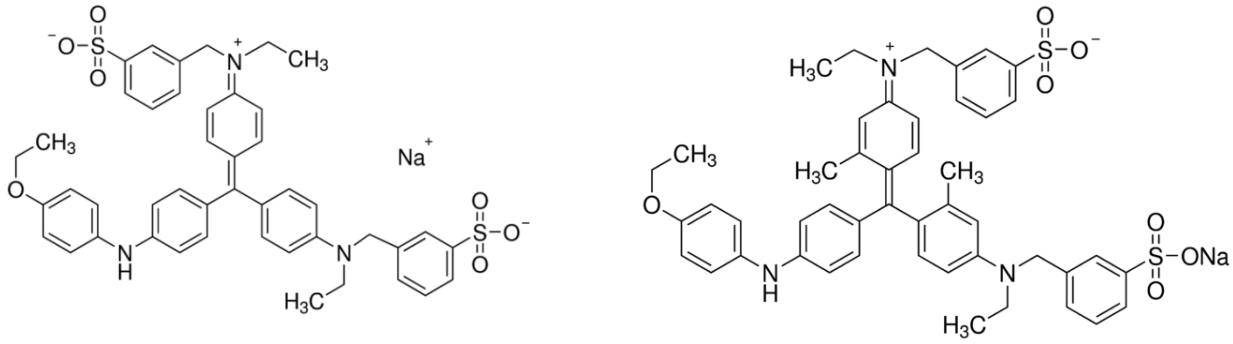

Figure 1.10 *Structures of BBR and BBG*

1.3.3.4. Difference between dyes and pigments

Based on physical and chemical properties, organic colorants are classified into two groups, dyes and pigments[54]. The main difference between the two is that, dyes are soluble in polar as well in non-polar solvents (water and organic solvents) while pigments are insoluble in both types of solvents. Actually, additional dispersants are added for the dispersion of pigments in water. The adsorption affinity of the dyes is selective while pigments can be adsorbed at the surface of any polymeric substrate. Both the reagents follow somewhat different adsorption mechanism. After adsorption, pigments can retain its original chemical structure while dyes lost its original chemical structure. The color of the dyes is because of have color bearing groups commonly known as chromophores which absorb light in the visible region of the solar spectrum. Most of the dyes have some additional groups called auxochromes (e.g.hydroxyl, amino, sulfonic and carboxylic groups) which help the

chromophores to absorb light. Moreover, dye represents a conjugated system which is stabilized by the phenomena of resonance.

1.3.3.5. Temperature effect on dye desorption from nanoparticles

The effect of temperature on dye desorption from nanoparticles can be investigated in the form of adsorption isotherms. The amount of adsorbate adsorbed on the surface of adsorbent at constant temperature is called adsorption isotherm. From the various adsorption isotherms it is clear that, at low temperature the adsorption affinity of the dye for nanoparticles increases with increase of temperature. However at high temperature this affinity decreases with rise of temperature.

1.3.3.6. Terminology of solar cell

1.3.3.6.1. Direct and indirect transition

The most important phenomenon occur in solar cells is the absorption of photons. So, on the bases of photon absorption, the semiconductors used in solar cells are classified into two types that are, direct and indirect semiconductors.

1.3.3.6.2. Direct transition

In such transitions absorption of photon leads to excitation from valence to conduction band and the material is known as direct semiconductors. In direct transition the momentum of electron-hole pairs remains constant. The momentum transfer to electron-hole pair is approximately zero, because photon has negligible momentum as result of very high speed of electromagnetic radiations. The mathematical expression for photon momentum is presented below.

$$\mathbf{P}_{\gamma} = \frac{\mathbf{h\omega}}{\mathbf{c}}$$

Whereas “c” represents velocity of the light, so

$$\boldsymbol{P_{\gamma} = P_h + P_e \approx 0}$$

$$\boldsymbol{P_h = -P_e}$$

According to the law of conservation of energy,

$$\mathbf{h}\omega = E_h + E_e \rightarrow (1)$$

Energy of exiton produced after photon absorption

$$E_h = \frac{Ph^2}{2\mathrm{m_h}} - E_v \quad \text{and} \quad E_h = \frac{Pe^2}{2m_e} + E_c \rightarrow (2)$$

By substitute equation 2 in equation 1, we finally get expression 3.

$$\mathbf{h}\omega = E_c - E_v + \frac{Pe^2}{2m_e} + \frac{Ph^2}{2\mathrm{m_h}}$$

$$\mathbf{h}\omega = E_G + \frac{P^2}{2}\left(\frac{1}{m_e} + \frac{1}{m_h}\right)$$

$$\mathbf{h}\omega = E_G + \frac{p^2}{2m_{com}} \rightarrow (3)$$

Equation 3 reveals that the energy momentum relationship for exiton is the same as that for electron in the conduction band. Photons with energy less than $E_G$will not absorbed. They will be transmitted or reflected if their energy is equal toE_G, however only those photons will be absorbed and cause excitation of electrons, which have energy greater than band gap energy.

1.3.3.6.3. Indirect transition

Another type of semiconductors called indirect semiconductors, for which the energy of photon is insufficient to excite an electron from the valence band to the conduction band. In order to excite the electrons, other particles like phonons or lattice vibrations take participations along with the absorption of photons. In other words transition is induced by the absorption of phonon. Although phonon is absorbed along with photon to create an exiton but there is possibility phonon emission after photon absorption. Both types of possibilities can be represented as,

In case of phonon absorption

$$\gamma + A^- \rightarrow \mathrm{h} + \mathrm{e}$$

$$P_{A^-} + P_\gamma = P_h + P_e$$

$$\mathrm{h}\Omega + \mathrm{h}\omega = E_h + E_e$$

In case of phonon emission,

$$\gamma \rightarrow \mathrm{h} + \mathrm{e} + A^-$$

$$P_\gamma = P_h + P_e + P_{A^-}$$

$$\mathrm{h}\omega = E_h + E_e + \mathrm{h}\Omega$$

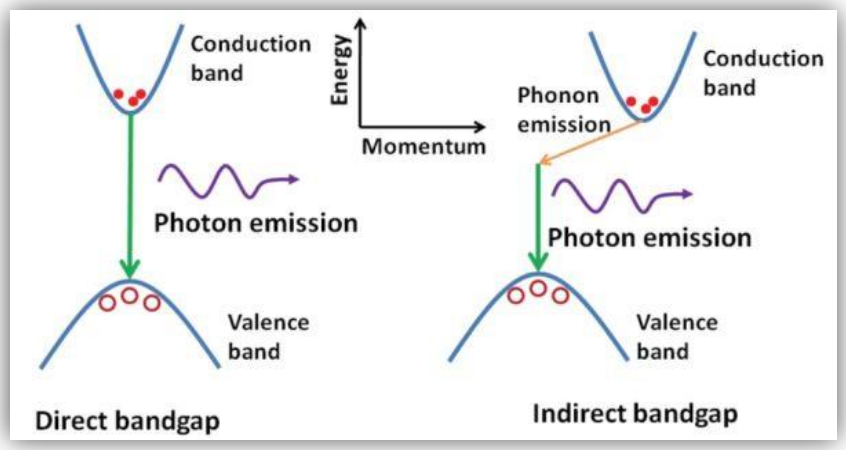

Figure 1.11 *Direct and indirect Transitions*

1.3.3.6.4. Air mass

A small portion of solar radiations are absorbed by the gaseous blanket around the earth. Low concentration gases e.g. methane, nitrous oxide, carbon dioxide, water vapours and various types of hydrocarbons absorb in the infrared region, while oxygen and ozone absorb radiation in ultraviolet region of the solar electromagnetic spectrum. Absorption depends upon the path length covered by the solar radiations in the atmosphere. More radiations will be absorbed if they cover a larger distance in the atmosphere. Let suppose, L_o represents thickness of the atmosphere and L is the distance covered by the solar radiation in the atmosphere then,

$$L = \frac{L_o}{\cos\theta}$$

Where θ represents the incident angle with the surface of the earth.

$$\frac{L}{L_o} = \frac{1}{\cos\theta}$$

The ratio of L to L_o is called air mass or air mass coefficient which represents the actual solar spectrum. The solar spectrum outside the atmosphere is represented by AMO, normal to the earth surface by AM1 and at angle 48° it is represented by AM1.5.

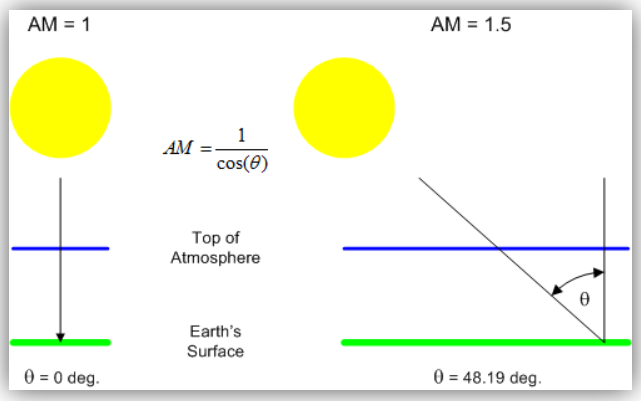

Figure 1.12 *Air mass*

1.3.3.6.5. Open circuit voltage

The maximum voltage across the solar cell when the flow of current in the external circuit is zero is called open circuit voltage. In photogenerated current, holes flow towards anode and electrons flow toward cathode due to its reverse biased nature. So, if a forward biased voltage is applied it will compensate and inhibit the flow of photogenerated current. With the increase of forward biased voltage, the flow of photogenerated current decreases and a point is reach at which current flow stops. The voltage at this point is called open circuit voltage represented by V_{oc}. Open circuit voltage indicates the extent to which recombination occur in the solar cell[55].

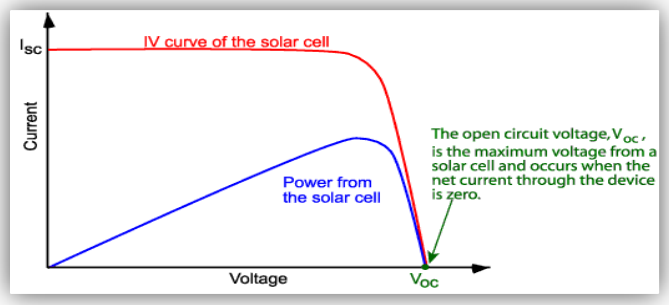

Figure 1.13 *Open Circuit Voltage*

1.3.3.6.6. Short circuit current

The maximum current extracted from a photovoltaic device when voltage across the device is zero is called short circuit current. Alternatively, it is the extracted current when there is a short circuit in the cell. It is represented by I_{sc} and its S.I unit is ampere [56]. Various terms like transport efficiency and carrier separation can be explained in the form of short circuit current density. Short circuit current depends upon the number of incident photons, optical properties like reflection and absorption, solar spectrum (AMO, AM1, AM1.5) and surface area of solar cells.

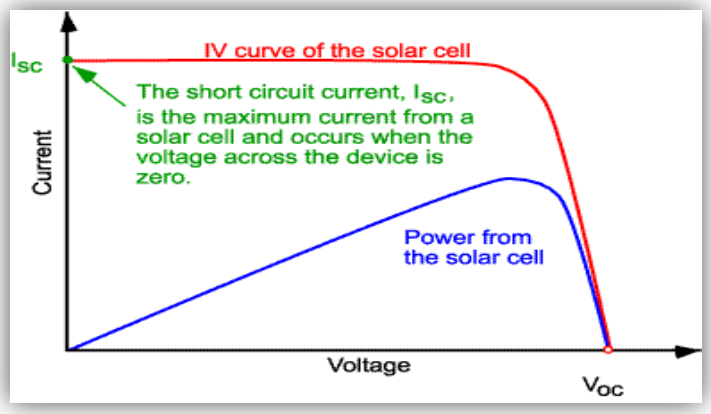

Figure 1.14 *Short Circuit Current*

1.3.3.6.7. Fill factor

At the given time the product of short circuit current and open circuit voltage is zero because at the given instant only one parameter have maximum value and the other will be zero and hence, maximum power will be zero. In order to explain the cell performance another term is introduced called fill factor represented by FF and mathematically can be written as,

$$FF = \frac{V_{max} \times I_{max}}{V_{oc} \times I_{sc}}$$

The theoretical value of fill factor is unity however its value ranges from 0.4 – 0.7. Moreover fill factor is dimensionless because it is a ratio between two similar parameters.

1.3.3.6.8. Efficiency

The fraction of incident power converted by a solar cell into electricity is called efficiency. It may be define as the ratio of output power to incident power from the sun. It is represented by $\boldsymbol{\eta}$ and mathematically it can be written as:

$$\eta = \frac{output\ power}{input\ power}$$

1.4 Literature review

Transition metals oxides are an encouraging alternative to replace silicon in silicon based solar cells, because they consist of low cost materials and have greater value of optical absorption coefficient. Besides the solar energy transformation, they also have applications in catalysis, electronics, gas sensors and magnetic storage media[57-59]. Among the different metals oxides, copper oxides $[CuO\ and\ Cu_2O]$ nanoparticles have attracted considerable attention as they are the most essential material for high efficient solar cells. However, as compare to other transition metal oxides such as, zinc oxide $[ZnO]$, tin dioxide $[SnO_2]$, titanium dioxide $[TiO_2]$ and iron oxides few reports are available on the preparation and characterization of copper oxide nanoparticles. Some common methods for the synthesis of copper oxide nanoparticles have been published recently for example sol-gel method [60], sonochemical technique [61], thermal decomposition of precursors [62], electrochemical method [63] and co-implantation of oxygen and metal ions[64], etc.

Copper oxide nanoparticles have narrow and direct band gaps of 2eV and 1.5eV respectively, this not only well matched with sun spectrum but also very close to the ideal band gap for solar cell[65].The maximum efficiency reported for cuprous oxide $[Cu_2O]$based solar cell is about 2%, under the condition of high temperature annealing and vacuum evaporation methods[66]. Solar cells comprising of cuprous oxide $[Cu_2O]$ and zinc oxide $[ZnO]$, fabricated by photo-and electrochemical deposition techniques have also been reported[67].

Although in most of the dye sensitized solar cells (DSSCs) cupric oxide $[CuO]$ has been used as a barrier layer and hole transfer layer, but few types of solar cells have been reported, in which cupric oxide $[CuO]$ was used as a p-type semiconductor[68].

T Okum *et al*. [69] fabricated thin films of cupric oxide $[CuO]$at different temperature ranging from 300℃ to 400℃, in order to study their photo-electrochemical properties. It was reported that the films deposited at 350℃ shows much better photo and electrochemical properties as compared to those films which were deposited at temperatures below or above 350℃.

R Sahay *et al*.[70] synthesized copper oxide nano-rods arrays and characterized for their composition morphology and growth conditions. These arrays of copper oxide $[CuO]$ nano-rods served as efficient hole-transport media for dye sensitized solar cells (DSSCs).

H Kidowaki *et al*. [71] fabricated nanoporous p-type copper oxide electrodes. They deposited different types of dyes on the surface of this electrode. Using these electrodes solar cells were fabricated and tested for their photovoltaic performance.

R Motoyoshi *et al*. [72] studied the effect of copper oxide $[CuO]$ barrier layer on zinc oxide $[ZnO]$ based dye sensitized solar cells (DSSCs) and their power conversion efficiencies were recorded. The solar cells were fabricated using zinc oxide as photo electrode, iodine tri-iodide solution electrolyte, Eosin-Y as sensitizer and platinum coated FTO glass as back electrode. The short circuit current density (J_{sc}), open circuit voltage (V_{oc}) and photovoltaic efficiency for the fabricated dye sensitized solar cells were assessed using radiant power of $100nWcm^{-2}$.

M H Habibia *et al.* [73] prepared a solar thermoelectric module for power creation from solar energy. They used different types of materials in this module but finally they observed that coating with copper oxide nanoparticles $[CuO]$ thin films elevated the temperature by 2℃ and voltage by 14.8%. This increased the efficiency of the cell by 10%, resulting in a 2.35% increase in overall output power.

Q Zhanga *et al*. [74] fabricated fullerene and copper oxides [CuO/C_{60} and Cu_2O/C_{60}] based thin film solar cells by spin-coating and electrodeposition techniques. In organic thin film solar cells, fullerene active layer has been used as n-type semiconductor, because it is a good electronic acceptor t oku. Electrodeposition is a technique for uniform thin layer formation and spin-coating is a low cost technique, which is crucial for any solar cell. They fabricated four different types of solar cells $[CuO_x/C_{60}]$ using electrodeposition and spin-coating techniques. These solar cells were characterized by current voltage measurement to find out their percent efficiency, under illumination at $100mWcm^{-2}$ using AM 1.5 solar simulator. It was concluded that cuprous oxide based solar cells [Cu_2O/C_{60}] fabricated by spin coating and electrodeposition methods provided much better power conversion efficiency compared to cupric oxide based solar cells [CuO/C_{60}].

K Rao *et al*.[75] synthesized and characterized copper oxide nanofibers. These nanofibers were then used as blocking layer in zinc oxide $[ZnO]$ based dye sensitized solar cells. The

photovoltaic performance of the fabricated dye sensitized solar cells (DSSCs) was investigated and increase of 25% was observed in the current density of these cells.

J Hou *et al.* [76] fabricated copper oxide $[CuO]$ based solar cells by depositing its thin film on ITO glass substrate. The performance of fabricated cell was investigated under illumination at $0.18 mAcm^{-2}$ and open circuit voltage (V_{oc}) of 0.04V were obtained.

Y Xu *et al.*[77] fabricated hybrid bulk heterojunction solar cells based on cupric oxide $[CuO]$ and cuprous oxide $[Cu_2O]$ with fullerene $[C_{60}]$ using ITO and FTO as substrates. The fabricated solar cells were characterized by current voltage measurement using AM 1.5 solar simulator.

M R Foroughi *et al.*[78] synthesized copper oxide nanorods under different experimental conditions and used as cathode. These nanorods were used in the fabrication of solar cell and characterized by current voltage measurement both dark and in light conditions. The efficiency of these cells were calculates in the range of 0.12- 0.29%.

1.5 Aims and Objectives

As describe in the literature review that initially copper oxide nanoparticles were used in the fabrication hybrid bulk heterojunction solar cells, but efficiency of these cells was very low ranging from 9×10^{-5} to 4.3×10^{-3}. Another problem associated with copper oxide $[CuO]$ nanoparticles is the band gap which absorbs light in the Ultra Violet (UV) region. To increase the efficiency of $[CuO]$ nanoparticles based solar cells and shift the absorption from Ultra Violet (UV) region to visible region of the light, we sensitized the copper oxide nanoparticles with brilliant blue red dye (BBR). In photosensitization we adsorb the brilliant blue red dye (BBR) on the surface of copper oxide nanoparticles.

For efficiency enhancement and better light harvesting, we fabricated a dye sensitized solar cell (DSSCs) using copper oxide nanohybrid material. We used copper oxide nanoparticles rather than bulk copper oxide because nanoparticles provide large surface area for the adsorption of dye during photosensitization. After fabrication the solar cell was characterized by current voltage measurement and observed maximum efficiency of 0.2%. The observed efficiency of DSSCs is hundred times greater than the efficiency of reported hybrid bulk heterojunction solar cells. In the fabrication of dye sensitized solar cell some conducting

polymers like P3HT and PEDOT:PSS were also used for various purposes like glass smoothing and making the flow of electrons in a single direction.

CHAPTER-02

EXPERIMENTAL

2.1 Chemical and reagents used

All the chemicals and reagents used in the synthesis of copper oxide nanoparticles and nanohybrid materials are listed in the table 2.1, which shows their chemicals formulas, molar mass and percent purity. As analytical grade chemicals were required for the synthesis of such type of materials, so all these chemicals and reagents were in their purest form and there was no need of further purification. The solutions of these chemicals were prepared in deionized and doubly distilled water.

Table 2.1:List of chemicals used in the synthesis of CuO and nanohybrid materials

S. No	compound	Chemical formula	Molar mass ($\frac{g}{mol}$)	Percent purity
1	Copper chloride	$CuCl_2$	134.5	≥ 99
2	Acetic acid	CH_3COOH	60	≥ 99
3	Sodium hydroxide	NaOH	40	≥ 99
4	Brilliant Blue red (Dye)	$C_{45}H_{44}N_3NaO_7S_2$	825.97	≥ 99
5	P3HT	$(C_{10}H_{14}S)_n$	54000-75000	≥ 99
6	PEDOT:PSS			≥ 99
7	Deionized water	H_20	18	≥ 99

2.2 Synthesis

2.2.1 Synthesis of copper oxide nanoparticles

Sol-Gel method was used for the synthesis of copper oxide nanoparticles. In the synthesis procedure the aqueous solution of copper chloride having concentration of 0.2M was mixed with 1 mL of glacial acetic acid. The resulting mixture was stirred at 100℃ for two hours. After that the aqueous solution of sodium hydroxide having concentration of 8M was added drop wise to the resulting mixture till the color of the mixture was turned dark brown. At this turning position the PH of the mixture was 7. Sodium hydroxide was used not only for changing the PH but also increases the rate of reaction taking place in the water. After some time the copper oxide nanoparticles were settled down which were washed with deionized water and dried.

$$CuCl_{2(aq)} + 2NaOH_{(aq)} \xrightarrow[100°C]{\text{Acetic acid}} CuO_{(ppt)} + 2NaCl_{(aq)} + 2H_2o$$

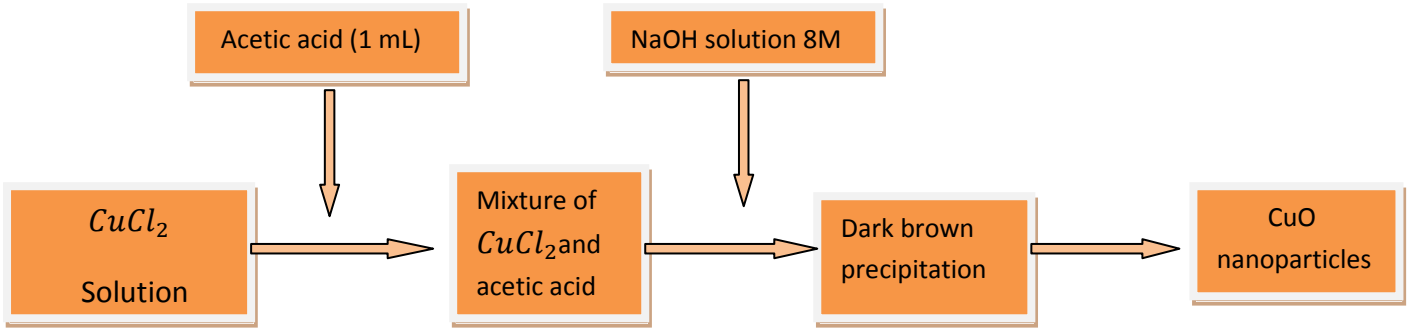

Figure 2.1 *Flow sheet represents the synthesis of CuO nanoparticles*

2.3 Sensitization of CuO nanoparticles with BBR dye

The surface of copper oxide nanoparticles were photosensitized by brilliant blue red dye. Before adsorption of the dye they absorb light in the ultra violet region (shorter

wavelength or higher energy) of the solar spectrum but after grafting the absorption region was shifted to the visible region (longer wavelength or lower energy). Moreover, we can use bulk copper oxide in the dye sensitized solar cells instead of nano CuO which absorb light in the visible region of the solar spectrum without dye adsorption, but electrolytic corrosion keeps their lifetime very short.

2.3.1 Preparation of Brilliant Blue Red dye solutions

The brilliant blue red dye is an organic dye used as sensitizer for the photosensitization of copper oxide nanoparticles. The solubility of BBR was examined in different solvents and it was confirmed that it is more soluble in the water which is a universal solvent. So its stock solution of 1mM was made in deionized water. From the stock solution, different solutions of dilute concentrations ranging from 15μM to 35μM were prepared and analyzed by UV-Visible spectroscopy.

Figure 2.2 *Solutions of different concentration of BBR Dye ranging from 15μM to 35μM*

2.3.2 Grafting of BBR on copper oxide nanoparticles (CuO)

The prepared dye solutions of different concentrations ranging from 15μM to 35μM were mixed with 1mg/ml of copper oxide nanoparticles at the ratio of 2mL : 2mL. The resulting mixtures were stirred at room temperature for 18 hours. After prolonged stirring the dye molecules were adsorbed chemically on the surface of copper oxide nanoparticles. Schematic representation of grafting is shown in Fig 2.3.

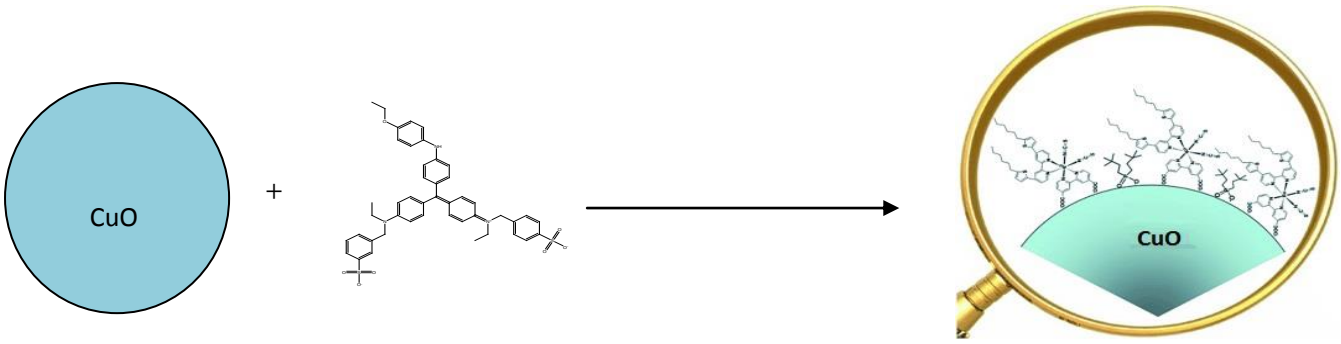

Figure 2.3 *Schematic representation of Grafting*

2.4 Characterization Techniques

During characterization the following important and basic instruments were used.

2.4.1 UV- Visible spectroscopic measurements

The optical properties or electronic absorption spectra of different materials were founded by using 1601- Shimadzu double beam spectrophotometer. As the sample and reference cells are expose to two different beams of light, so it is called double beam spectrophotometer. The detector takes the ratio after detection of the reference and the sample beam alternatively and after processing the data readout by computer. Quartz cells of 1 cm thickness were used for holding the sample during its analysis by UV-Visible spectrophotometer.

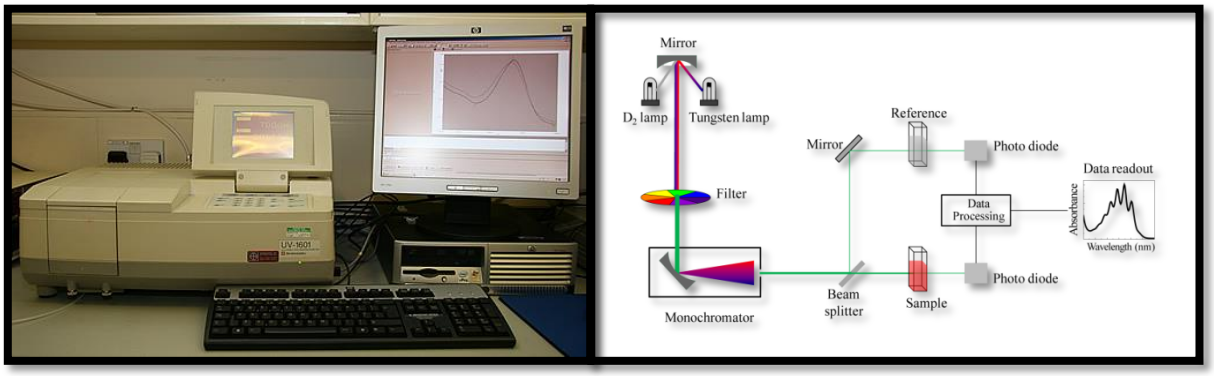

Figure 2.4 *UV-Vis Spectroscopy*

2.4.2 X-rays powder diffraction (XRD)

XRD is an analytical technique used for the determination of average crystallite size, unit cell dimension, phase identification and measurement of percent purity in the sample. The fundamental principle of XRD is based upon the bragg's law ($n\lambda=2d\sin\theta$). The three basic components of X-ray diffractometer are a sample holder, an X-ray tube and a detector. Firstly electrons are produced by heating a filament and accelerating these electrons towards

the target material. The accelerated electrons eject the electrons from the inner shell of the target material. In order to fulfill this deficiency electron from higher energy level jump to the lower energy level by emitting some type of radiations called X rays. Before passing through the sample, they are passes through a monochrometer to produce monochromatic X-rays which is required for diffraction analysis. Although different materials are uses as target material but the most commonly used material is the copper. After that they are passes through the sample, detected by the detector and readout by the computer.

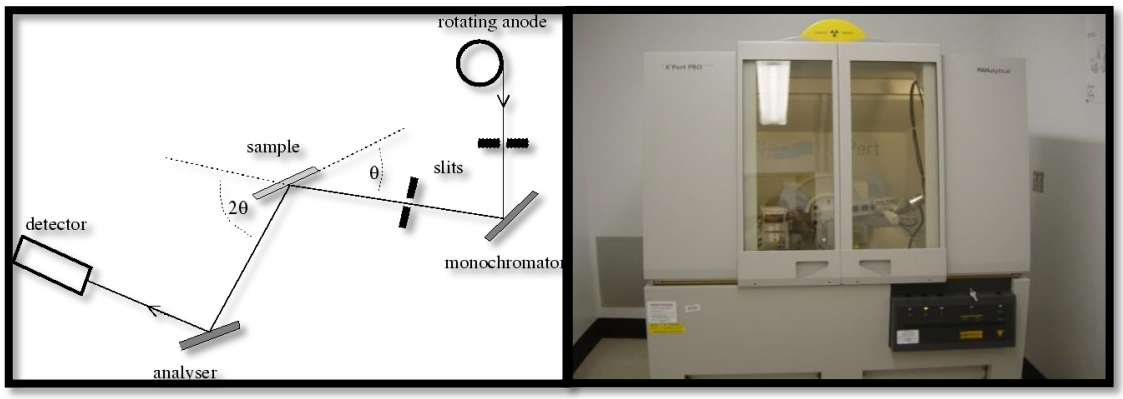

Figure 2.5 *X-Ray Diffractometer*

2.4.3 Fluorescence and fluorescent instrumentation

When a molecule is excited to the higher energy state by absorbing a photon in the UV-Visible region of the spectrum, then the excited molecule comes to its ground state by emitting that photon with longer wavelength. This phenomenon is known as fluorescence which takes place in very short time about 10^{-9}sec. As the emitted radiations have longer wavelength than the absorbed radiation, so this change in wavelength is called stokes shift.

The three basic components of a fluorescence instrument are light source, sample holder and a detector. The light source emits light in the visible region of the solar spectrum and passes through the excitation monochromater. The monochromater transmits the light selectively and then passes through the slits, where further filtration of the light occurs. The filtered beam of light is passes through the sample solution, absorb by fluorphors of the sample and causing fluorescent emission. The emitted light then passes through emission monochromater, slits and finally detected by the detector.

There are some advantages of fluorescent method over absorption spectroscopy.

1) In fluorimetry two wavelengths (excitation and emission) are used instead of one wavelength as in absorption spectroscopy.
2) In fluorimetry there is low signal to noise ratio as compare to absorption spectroscopy.
3) The third advantage of fluorimetry over absorption spectroscopy is because of its greater range of linearity.

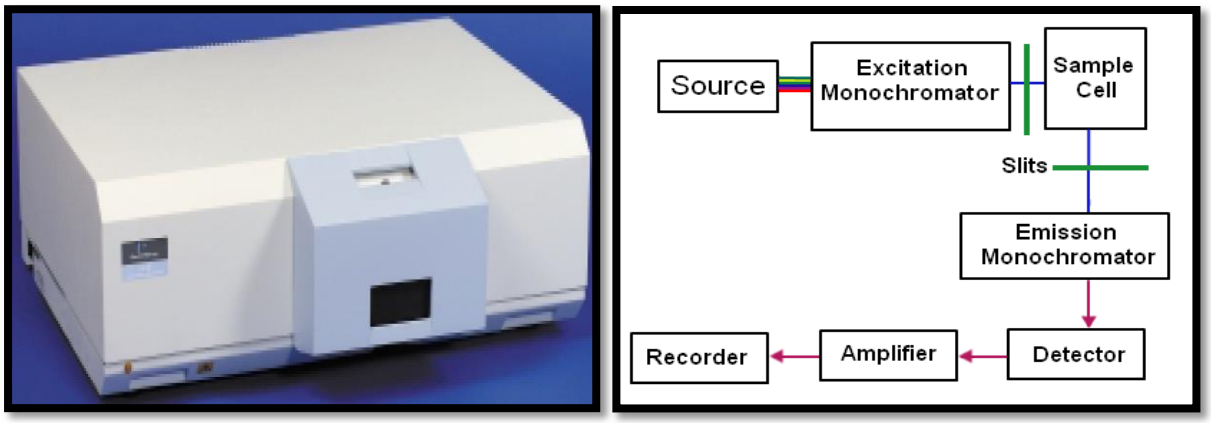

Figure 2.6 *Fluorometer*

2.4.4 FT-IR spectroscopic measurement

FT-IR stands for Fourier Transform Infrared Spectroscopy. As a specific chemical bond interacts with IR radiations in the specific region to give a characteristic band, so this technique was used to find out the possible groups present in the synthesized copper oxide nanoparticles. With the help of this technique we also conform that whether the dye molecules adsorb on the surface of copper oxide nanoparticles or not. FTIR spectrometer consist of a light source, two mirrors (one is fixed and the other is moveable), a beam splitter and an infrared detector. The basic part of the FTIR spectrometer is the beam splitter which transmits half of the incident light and reflects the remaining half. The reflected part travels to the fixed mirror while the transmitted portion travels to the moving mirror. The two beams are reflected by both the mirrors towards the beam splitter where each of the two beams is again half transmitted and half reflected in such a way that one travels to the source and the other to the detector after passing through the sample.

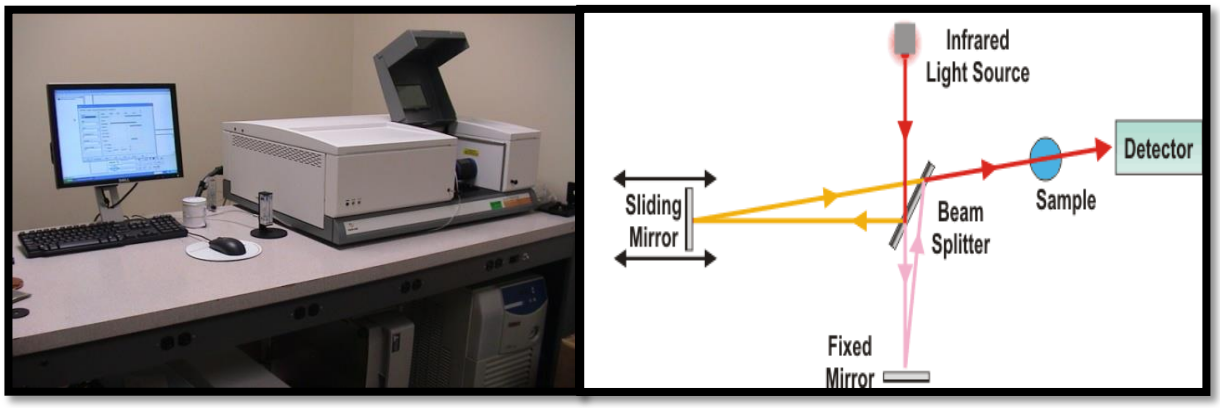

Figure 2.7 *FT-IT Spectrometer*

2.5 Fabrication of Dye Sensitized Solar Cell (DSSC)

2.5.1 Preparation of P3HT solution

20mg/mL solution of *P*3HT was made by dissolving its 80mg in 4 mL chloroform. The solubility of *P*3HT was further increased by heating the mixture at 60℃ for 15-20 minutes in inert atmosphere. This solution was labeled asS_1. Another solution of the hybrid material having concentration 1mg/mL was made and named as S_2. Then equal volumes of both the solutions were mixed in order to prepare the active later of copper oxide nanoparticles.

2.5.2 Substrate selection and treatment

Indium doped tin oxide coated glass sheets were used as substrate material in the dye sensitized solar cells. The dimension of the glass was $3 \times 2\ cm^2$ while thickness of the conducting layer of ITO was 80 nm. The substrate was labeled into two parts, smaller and larger. The larger part was covered with scotch tape while the smaller was exposed to dilute HCL in order to remove its conducting ITO layer. After ITO removal from the smaller part, the substrate was washed with distilled water and left for several hours to get dried. The tapes were removed from dried sheets and washed with acetone.

2.5.3 Deposition of PEDOT.PSS over glass sheet

To remove the roughness of the glass, a thin layer of conducting polymer PEDOT.PSS was deposited on the surface of glass sheets. As PEDOT.PSS is a p-type polymer, so it was used not only to remove the roughness of the sheets but it is also very

helpful in holes transportation towards the conducting layer of the glass (ITO). The thin layer of the conducting polymer was deposited by using spin coater. During spin coating a small drop of PEDOT.PSS solution was placed at the center of glass sheet and then spinning the sheet at the rate of 5000rpm. The drop of solution was spread on the surface of glass sheet, because of centripetal acceleration. Fume exhaust, centripetal acceleration and rotational speed can affect the properties of the film.

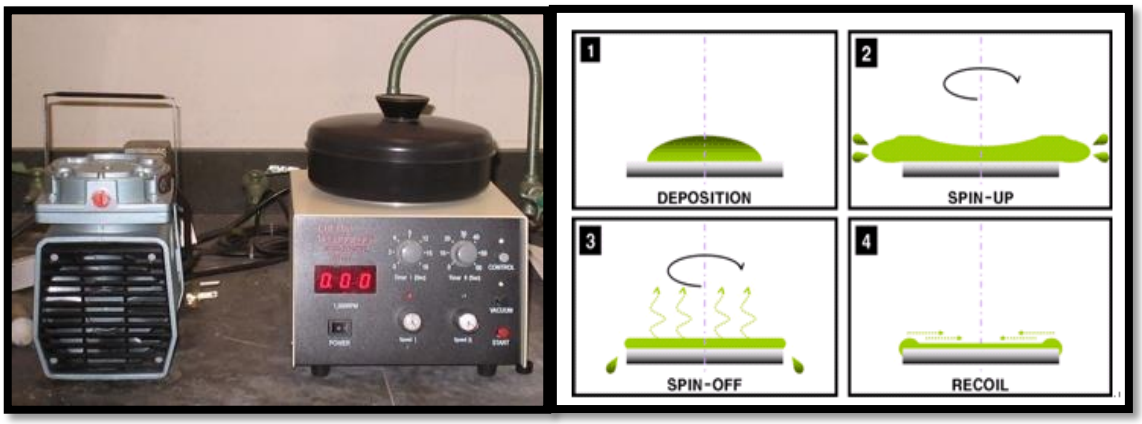

Figure 2.8 *Sppin Coater*

2.5.4 Deposition of active layer

The mixture of a conducting polymer P3HT and dye sensitized copper oxide nanoparticles at the ratio of 3:7 respectively is called active material. A thin layer of active materials was deposited on PEDOT.PSS coated glass substrate with the help of spin coater. Initially the spin coater was run at the rate of 1500 rpm for 20 mints in the next 20 mints it was run at the speed of 500rpm. Repeating the spinning at the rate of 500 rpm was continued in order to remove the remaining solvent which greatly reduces the efficiency of solar cells.

2.5.5 Deposition of Aluminum metal (As cathode)

A thin cathodic layer of aluminium metal was deposited by thermal evaporation under high vacuum conditions. Deposition of Al was performed in the metal evaporator and 80 nm thick cathodic contacts were made to extract and guide electrons to the external circuit. The last step of fabrication process was the annealing of the device. The device was annealed at 90°C for 15 minutes under argon flow to achieve nice morphological distribution of the

active blend. Then the cells were cooled under argon flow for 15 minutes at the mouth of the sintering glass tube being covered with a dark cloth. The nanohybrid dye sensitized bulk heterojunction device was thus ready for characterization with the following shape.

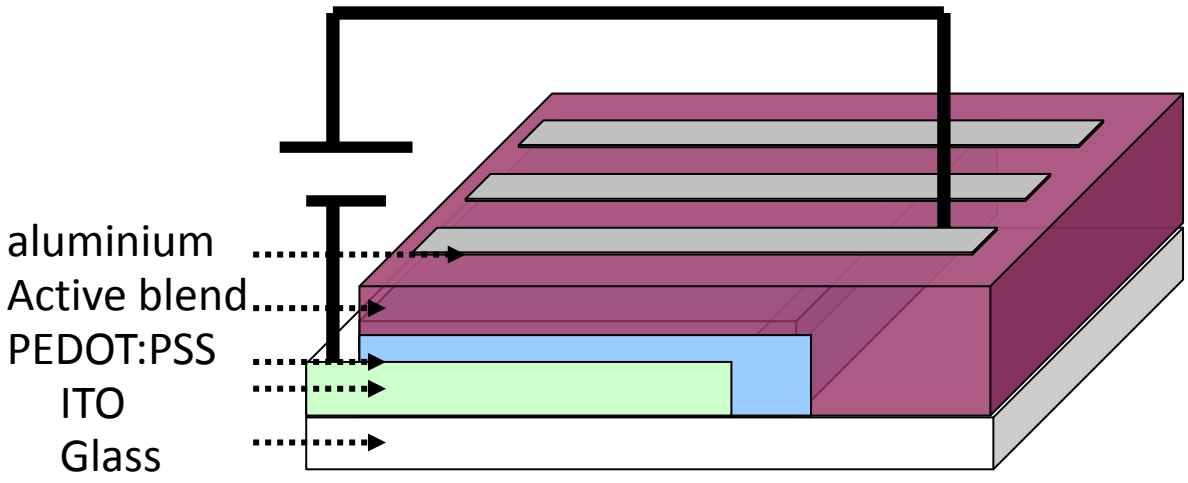

Figure 2.9 *Commercial Solar cell*

2.5.6 Solar simulator (xenon light source)

Solar simulator also called artificial sun is an instrument which imitates the solar spectrum and irradiance. Although this device uses xenon arc lamp as light source, however every xenon light source is not a simulator but every simulator is a xenon light source. According to international standard, the intensity of the light beam emitted by xenon lamp in solar simulator under AM1.5G condition should be 1000w/m^2. This intensity is known as one sun. Beside the xenon lamp the simulator also consist of reflectors, integrator lens, collimating lens, shutter, mirrors and light feedback and control. On the bases of spectral match, stability and non-uniformity of the light beam the solar simulator are classified into three classes: class A, class B, and class C. The stability and non-uniformity should be in sequence as class A $<$ 2%, class B $<$ 5% and class C $<$ 10%.

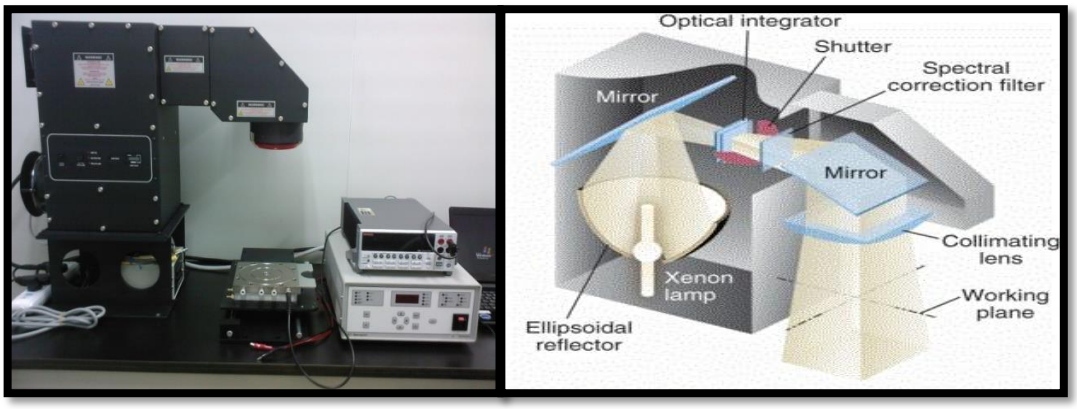

Figure 2.10 *Solar Simulator (Artificial Sun)*

CHAPTER-03

RESULTS AND DISCUSSION

Copper oxide (CuO) nanoparticles were successfully synthesized by sol-gel method already discussed in the experimental section. The synthesized nanoparticles were characterized by employing various techniques followed by its fabrication using Brilliant Blue Red (BBR) dye as photosensitizer for harvesting solar energy.

3.1 Optical and morphological properties of CuO nanoparticles

Optical and morphological properties of CuO were determined using the following characterization techniques:

- UV-Visible spectroscopy
- Fluorescence spectroscopy
- X-Rays diffraction analysis
- Fourier Transform Infrared (FT-IR) Spectroscopy
- Scanning electron microscope

3.1.1 Optical Properties

3.1.1.1 UV-Visible Spectroscopy

The absorption spectrum of the synthesized copper oxide[CuO] nanoparticles were logged using UV-Visible spectrometer. The wavelength range of incident light was from 300 nm to 800 nm. UV-Vis spectrograph was recorded to calculate band gap energy of [CuO] nanoparticles. UV-Vis spectrograph is shown in the Fig 3.1. Maximum absorption band was observed at 303 nm which was found in agreement with the literature. Hui Wang *et al* reported maximum absorption band at 340 nm [64].

As UV-Vis spectrograph was recorded to find out band gap energy, it was calculated from band edge by extrapolating the graph to where the absorption is initiated.

The band gap energy of 2.13 eV was calculated from band edge lies at 582 nm. The band gap energy of bulk copper oxide is 1.85 eV. The blue shift in band gap energy of bulk and CuO nanoparticles is because of quantum confinement effect which confined the electrons to

potential wells. Moreover, the formation of nanoparticles was indicated by blue shift in band gap energy.

To find out the band gap energy the following equation was used

$$E_g = \frac{hc}{\lambda}$$

Where

E_g = Band gap energy in eV

c = Speed of light (3×10^{10} cm s^{-1})

h = Plank's constant ($4.135667516 \times 10^{-15}$eV s)

λ= Wavelength of the emitted radiation.

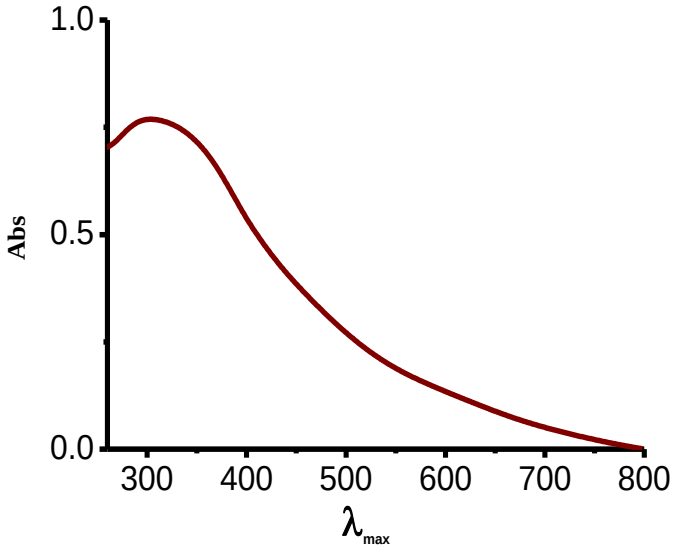

Figure 3.1 *UV-Vis Absorption Spectrum of CuO nanoparticles*

3.1.1.2 Characterization by Fluorescence emission spectroscopy

The photoluminescence spectrum of the synthesized copper oxide nanoparticles excited at 320 nm is shown in the Fig 3.2. It is observed that CuO nanoparticles shows three broad emission peaks at 425 nm, 488 nm and 538 nm, respectively. The first broad and intense peak is due to band edge emission, the second one corresponds to some artifacts while the third one results from excitons recombination in the valence band because of singly ionized oxygen vacancy. The emission at 425 nm shows 122 nm stokes shift if we compare it with UV-Visible spectrum which shows maximum absorption at 303 nm[79].

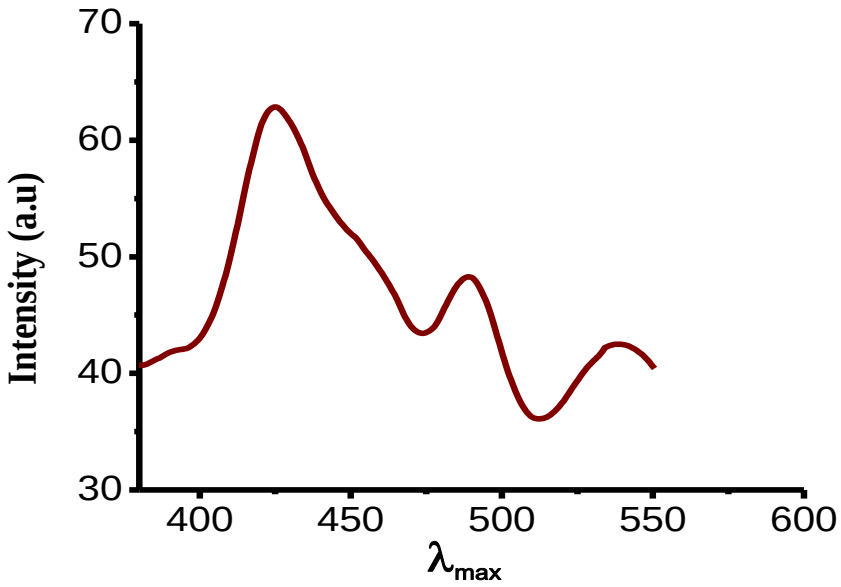

Figure 3.2 *Photoemission Spectrum of CuO nanoparticles*

3.1.2 Morphological Properties

3.1.2.1 Powder XRD diffraction analysis

XRD pattern of the synthesized copper oxide nanoparticles is shown in the Fig 3.3. The intense and sharp diffraction peaks in the X-rays diffractogram shows that the synthesized copper oxide nanoparticles retained its crystalline monoclinic structure. The lattice parameters for corresponding monoclinic structure are a = 4.65Å, b = 3.14Å, 5.12Å, α = 90°, β = 99°, γ = 90° and V = 80Å which match well with the literature values. Moreover, no extra peaks rather than CuO were observed, which indicates the purity of the synthesized copper oxide nanoparticles. The nanoscale size was investigated from peaks broadening in the diffractogram. Using Debye sherrer's equation, average crystallite size of 13 nm was calculated.

$$S = \frac{\kappa\lambda}{\beta \cos\theta}$$

Where

S = Crystallite size

β =Full width at half maximum (FWHM)

θ =Bragg's angle

k = dimensionless shape factor.

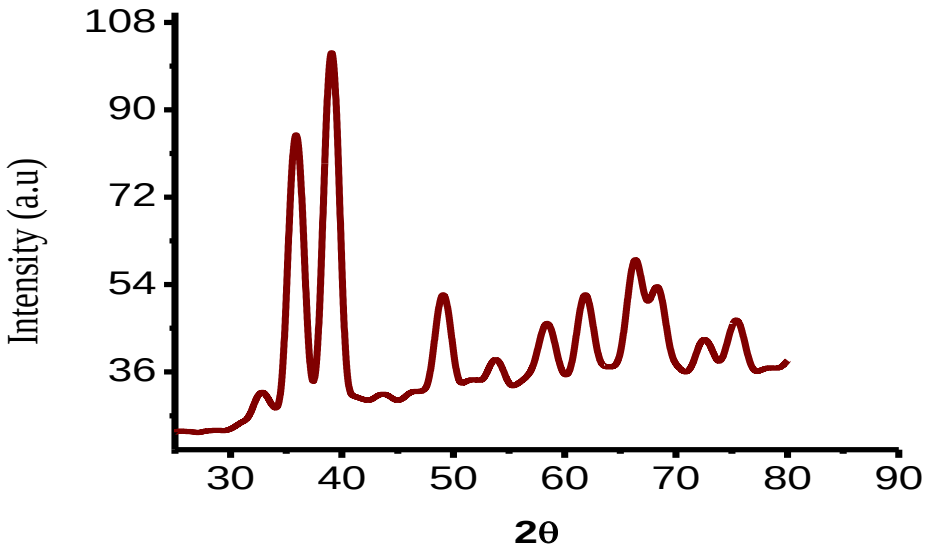

Figure 3.3 *XRD pattern of CuO nanoparticles*

Table 3.1 *: Parameters obtained from XRD data for the calculation of average particle size.*

S.No	Position(2θ)	θ	(θ) radian	Cos θ	β(degree)	βradian	Crystallite size
1	32.8	16.4	0.2862	0.99	0.3542	0.006	23.3
2	35.9	17.9	0.31	0.99	0.4723	0.008	17.5
3	39.0	19.5	0.34	0.99	0.5314	0.009	15.5
4	49.1	24.6	0.42	0.99	0.5904	0.01	14.0
5	53.9	29.9	0.52	0.99	0.7085	0.012	11.6
6	58.4	29.2	0.50	0.99	0.7085	0.012	11.6
7	61.9	30.9	0.53	0.99	0.7085	0.012	11.6
8	66.5	33.3	0.58	0.99	0.7085	0.012	11.6
9	68.2	34.1	0.59	0.99	0.5904	0.01	14.0
10	72.6	36.3	0.63	0.99	0.7085	0.012	11.6
11	75.3	37.7	0.66	0.99	0.864	0.015	09.3

3.1.2.2 Scanning Electron Microscopy

The surface morphology of copper oxide nanoparticles (CuO), synthesized by sol-gel method were studied by scanning electron microscopy (SEM) running at 20 kV. The SEM images of CuO nanoparticles on various scales are shown in the Fig 3.4 (a), (b) and (c). The SEM images show that most of the particles having size of 1μm and 2 μm.

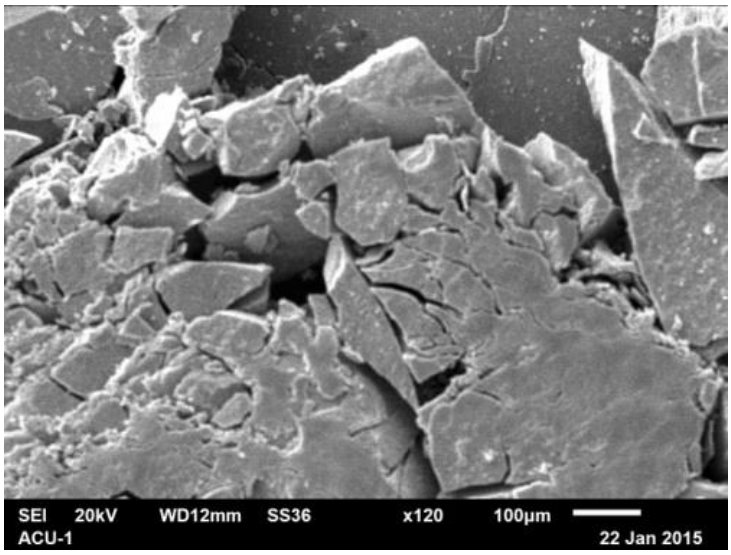

Figure 3.4 (a) *SEM image of CuO nanoparticles*

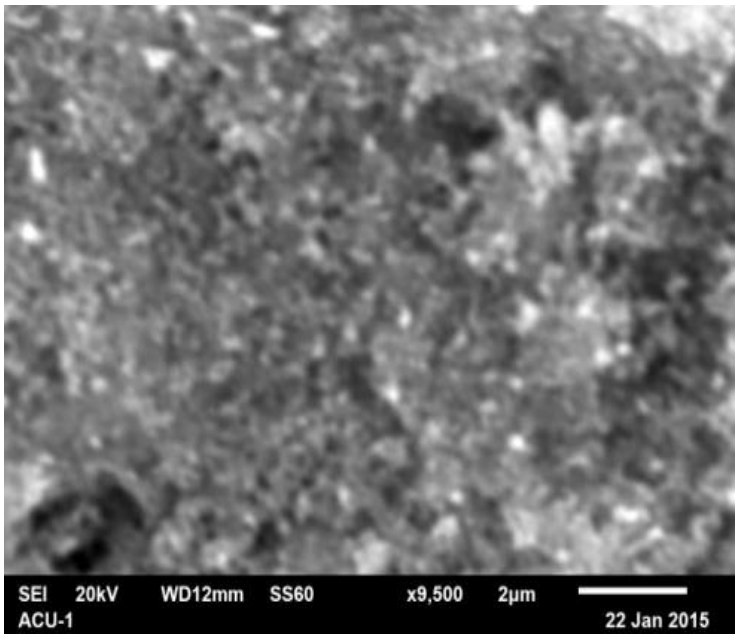

Figure 3.4 (b) *SEM image of CuO nanoparticles*

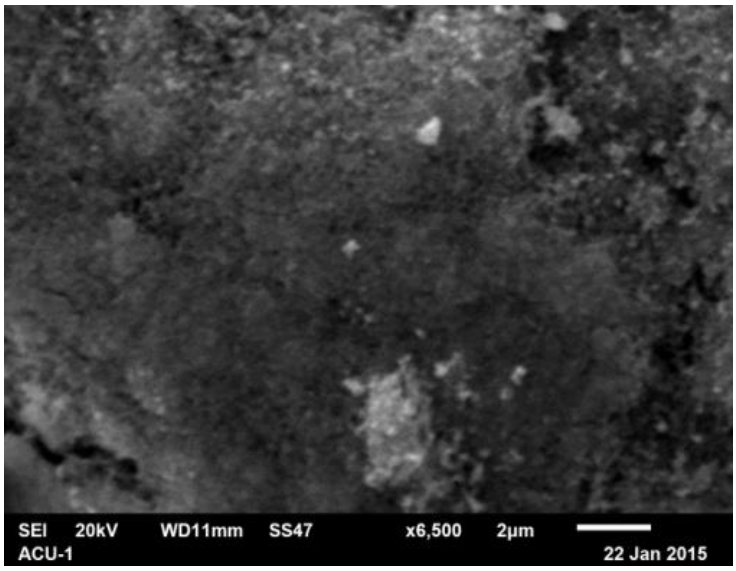

Figure 3.4 (c) *SEM image of CuO nanoparticles*

3.1.2.3 Energy- dispersive X-Ray analysis

For elemental analysis an analytical technique called as energy-dispersive X-Ray spectroscopy (EDX or EDS) was employed. The EDX spectrum of the synthesized copper oxide nanoparticles is shown in the Fig 3.5. The EDX spectrum shows that besides the Cu and O elements some traces of carbon impurities are also detected. Moreover, the weight% of copper, oxygen and carbon evaluated from EDX is 75.40%, 21.23% and 3.37% respectively. The calculated weight ratio of Cu and O is 3.55, which is near to the actual value of 4 for cupric oxide. The EDX results verified that the synthesized powders are copper oxide nanoparticles, which is in resemblance with XRD results.

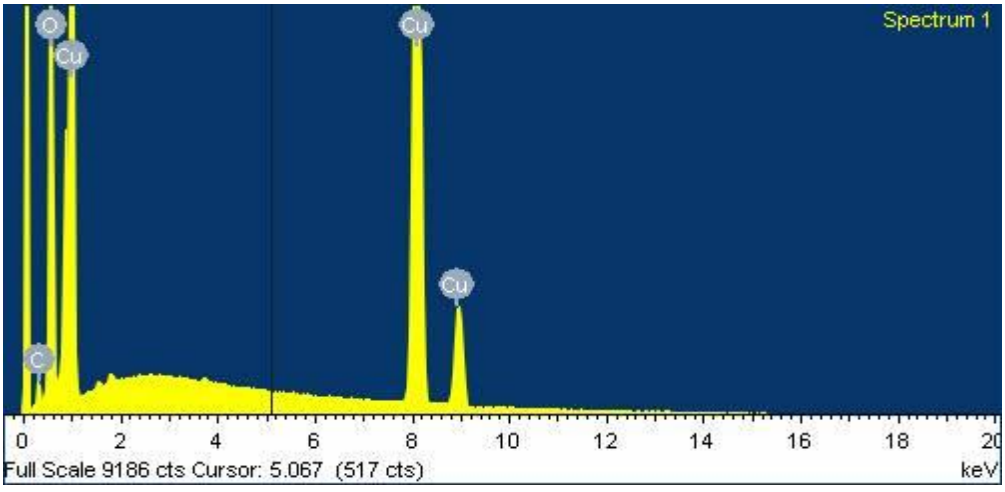

Figure 3.5 *EDX Spectrum of CuO nanoparticles*

3.1.2.4 Characterization by FT-IR spectroscopy

The successful synthesis of copper oxide nanoparticles (CuO) was also confirmed by Fourier Transform Infrared Spectroscopy commonly abbreviated as FT-IR. The FT-IR spectrum of the CuO nanoparticles is shown in the Fig 3.6. The presence of the sharp peak at $520\,cm^{-1}$ is characteristic peak of Cu-O stretching vibrations. The peak at $827\,cm^{-1}$ is because of C-Cl stretching while peaks at $1361\,cm^{-1}$ and $1473\,cm^{-1}$ can be attributed to bending of CH_3 group in different dimensions. The peaks positioned at $3379\,cm^{-1}$ and $1645\,cm^{-1}$ attributed to stretching and bending of O-H bond in water molecules. The characteristic peak positioned at $520\,cm^{-1}$ confirmed the successful synthesis of copper oxide nanoparticles.

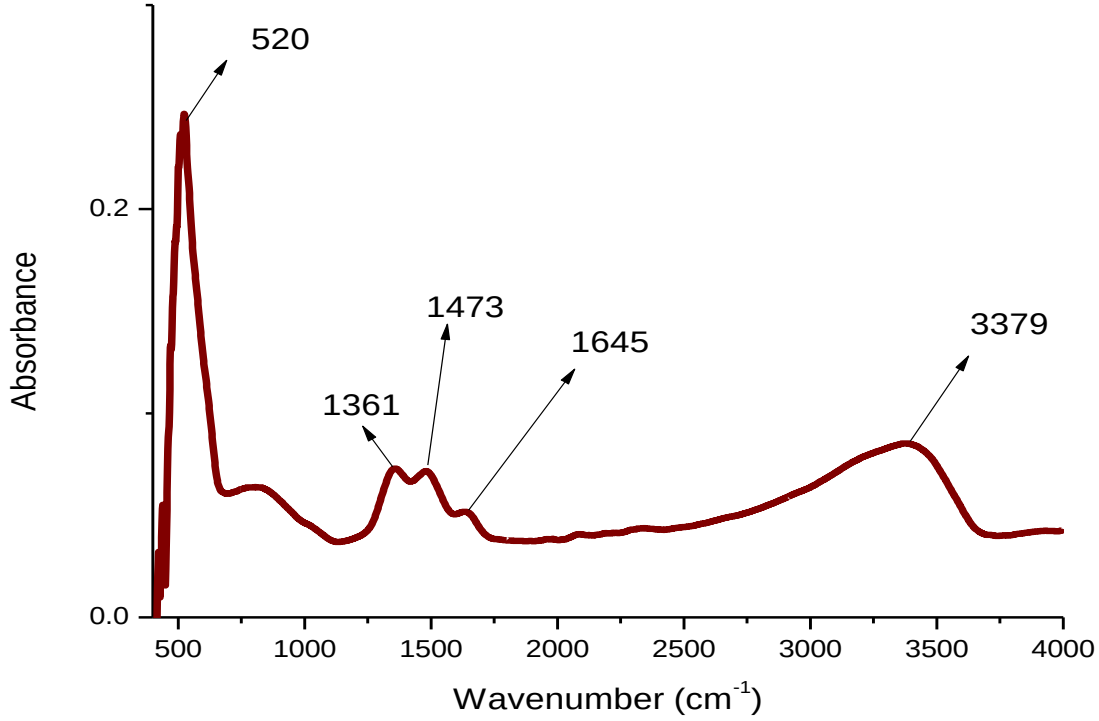

Figure 3.6 *FT-IR spectrumof CuO nanoparticles*

3.2 Optical study of BBR dye

3.2.1 Characterization by UV-Visible spectroscopy

The UV-Visible spectrum of the brilliant blue red (BBR) dye, used for the sensitization of copper oxide nanoparticles is shown in the Fig 3.7. The dye shows maximum absorption at 551 nm and two small peaks at 260 nm and 309 nm. The broad and intense peak at 551 nm is because of n-π^* transition of lone pair of electron present in sulphonic group

attached to the benzene ring in dye molecules. The two small peaks at 260 nm and 309 nm are because of π-π^*transition of delocalized electronic cloud of aromatic rings.

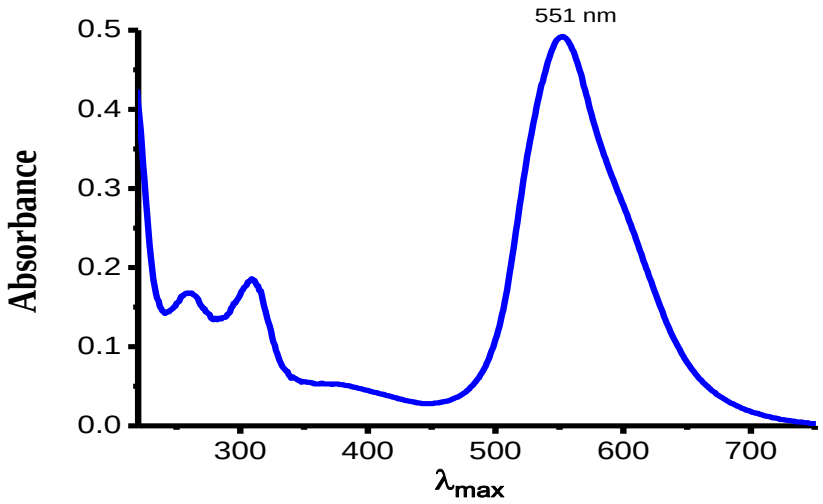

Figure 3.7 *UV-Vis Spectrum of BBR Dye*

3.2.2 Characterization by fluorescence emission spectroscopy

The emission of radiation particularly in the visible region of the spectrum, from a substance that is excited by incident radiations is called fluorescence. The fluorescence occurs in nanoseconds because the excited species have finite time usually ranges from 1-10 nanoseconds. The emitted light has lower energy or longer wavelength than absorbed light because of energy dissipation during vibrational relaxation of the excited species. The BBR dye was excited at 571 nm, 20 nm onward than absorption peak which was at 551 nm. The emission spectrum observed is shown in the Fig 3.8. The dye shows maximum emission at 693 nm.

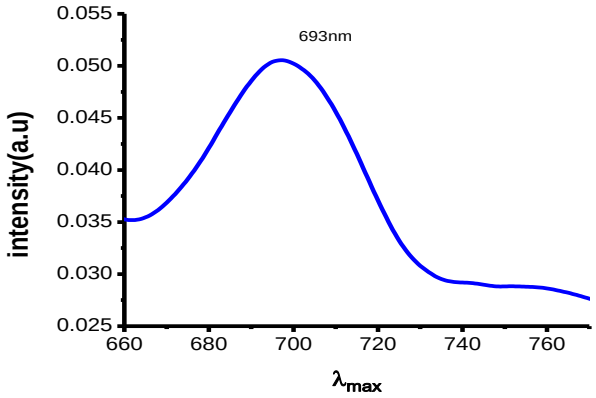

Figure 3.8 *Fluoresce emission Spectrum of BBR Dye*

3.3 Optical study of Hybrid material (CuO + BBR)

3.3.1 Characterization by UV-Visible spectroscopy

The hybrid material was prepared, when dye molecules of BBR were adsorbed on the surface of copper oxide nanoparticles. The dye adsorbed at the surface of CuO due to the presence of two sulphonic groups which acted as anchoring groups. Firstly, the hybrid material (CuO + BBR) was characterized by UV-Visible spectroscopy and the UV-Visible spectrum of the hybrid material is shown in the Fig 3.9. In Fig 3.10, the presence of the peaks both of the dye and copper oxide clearly indicates the adsorption of dye molecules to the surface of copper oxide nanoparticles. Moreover when we compared it with the UV-Visible spectrum of the dye, then the 19 nm blue shift and the absence of two small peaks of the dye further verified the adsorption process. The electronic transition occurs at higher energy in the hybrid material due to electrostatic interaction between CuO nanoparticles and dye molecules leading to a blue shift of 19 nm.

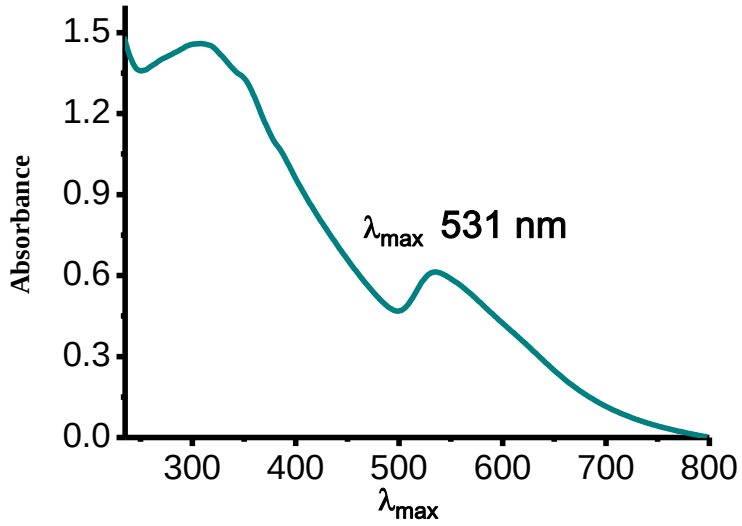

Figure 3.9 *UV-Vis Spectrum of Hybride material (CuO + BBR Dye)*

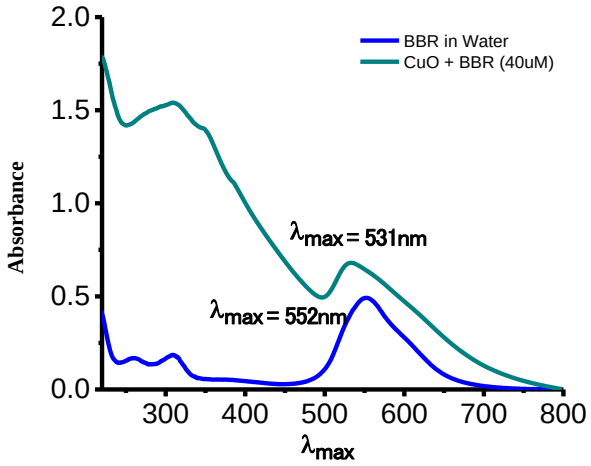

Figure 3.10 *UV-Vis Spectrum of BBR and Hybride material (CuO + BBR Dye)*

3.3.2 Characterization by fluorescence spectroscopy

Further confirmation, of adsorption of dye on the surface of copper oxide nanoparticles was done using fluorescence emission spectroscopy. The Fluoresce emission spectrum of the hybrid material is shown in the Fig 3.11 shows maximum emission at 693 nm when it was excited at 571 nm. Comparison of emission spectrum of the hybrid material with dye shows increase in intensity of the hybrid material and 3 nm blue shift. Change in intensity and blue shift verifies the adsorption of dye molecules on the surface of copper oxide nanoparticles. The fluorescence emission study not only supports the results of UV-Visible spectroscopy, but it also suggests electron transfer from copper oxide nanoparticles to the dye thereby increasing its intensity.

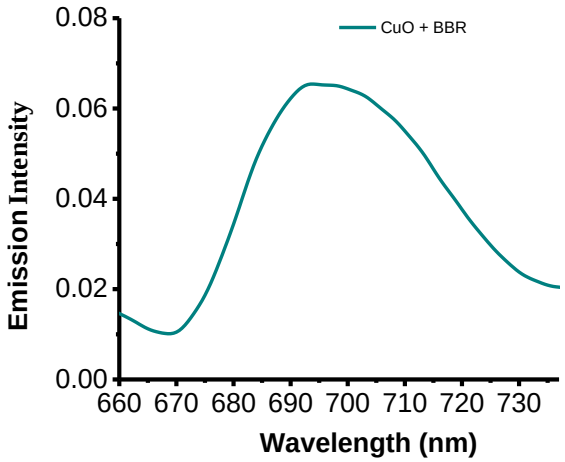

Figure 3.11 *Emission spectrum of Hybride material (CuO + BBR Dye)*

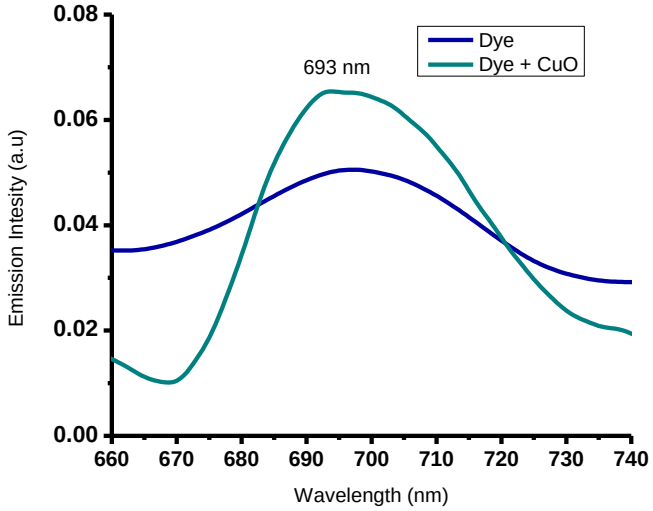

Figure 3.12 *Emission spectrum of BBR and Hybride material (CuO + BBR Dye)*

3.4 Current voltage measurement

In the pattern of commercially available dye sensitized solar cell (DSSCs), we fabricated a solar cell based on dye sensitized copper oxide nanoparticles. During fabrication, a conducting polymer poly(3,4-ethylenedioxythiophene) polystyrene sulfonate (PEDOT:PSS) was deposited over the conducting glass (ITO). While the conducting layer of polymer was covered by the active layer of BBR dye sensitized copper oxide nanoparticles containing poly(3-hexylthiophene-2,5-diyl) (P3HT). A cathodic layer of Aluminum was deposited over the active layer. After fabrication the cell was exposed to current-voltage characterization in order to find out the different parameters like short circuit current density (J_{sc}), open circuit voltage (V_{oc}), fill factor (FF) and maximum power point (M_{pp}). On the basis of these parameters we calculated the percent efficiency (η%) which describes the workability of a solar cell.

3.4.1 I-V characterization of CuO based solar cell

The I-V curves of copper oxide nanoparticles CuO based solar cells at the different concentration of the dye ranging from 25 μM to 40 μM is shown in the Fig 3.13. The black curve represents that copper oxide nanoparticles containing P3HT shows no current under the condition of dark. But, when they were exposed to the light, electrical current was produced as shown by the red curve. Moreover, the increase in current density was observed when BBR dye was used as photosensitizer for CuO nanoparticles. Maximum current density was

observed when concentration of BBR was taken 30μM. By further increasing the dye concentration the current density was decreased, because at high concentration accumulation of dye molecules occur on the surface of copper oxide nanoparticles.

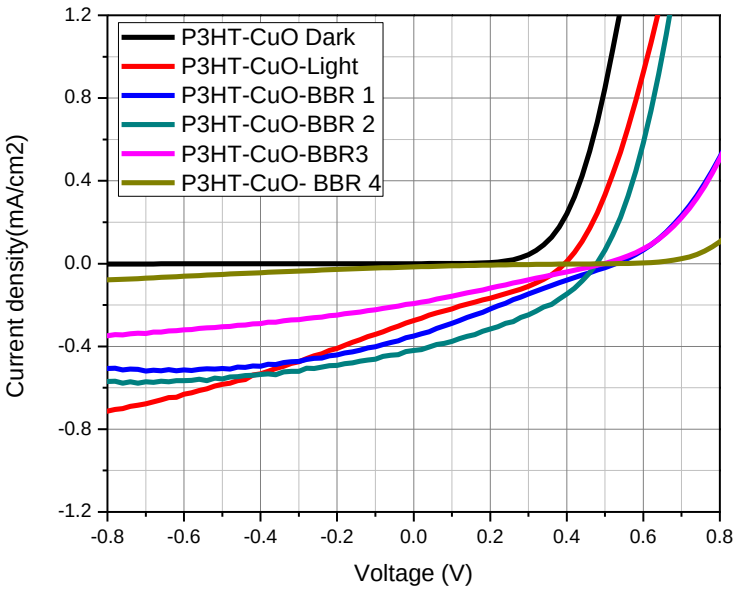

Figure 3.13 *I-V curves of copper oxide nanoparticles based solar cells at the different concentration of the dye*

The various parameters calculated from I-V measurement are shown in the table 3.2. The tabulated data shows that initially short circuit current density increases with increase of dye concentration up to the concentration of 30μM. The corresponding efficiency of the cell also increases and maximum efficiency of 0.1% was achieved at the concentration of 30μM. So this concentration of dye is the optimum concentration at which the hybrid material has maximum efficiency. The table also shows the effect of dye concentration on other parameters like short circuit current, open circuit voltage and fill factor.

Table 3.2 : *Parameters obtained from I-V measurement curves*

Device Composition	J_{sc} (mA/cm^2)	V_{oc} (V)	M_{PP} (mW/cm^2)	Fill factor	Efficiency (η %)
P3HT-CuO light	0.28	0.39	0.035	0.32	0.04
2.5×10^{-5} M BBR-CuO	0.35	0.53	0.046	0.25	0.05
3×10^{-5} M BBR- CuO	0.42	0.47	0.074	0.38	0.1
3.5×10^{-5} M BBR- CuO	0.19	0.49	0.025	0.27	0.03
4.0×10^{-5} M BBR- CuO	0.02	0.51	0.0014	0.14	0.001

3.4.2 Effect of concentration on short circuit current density

Short circuit current is the maximum current that can be extracted from a solar cell. The effect of dye concentration on short circuit current density is shown in the Fig 3.14. Initially short circuit current density increases with increase of dye concentration up to 30μM, but beyond this concentration short circuit current density decrease, because aggregation of dye molecules occurs on the surface of copper oxide nanoparticles which increases the chances of charge recombination.

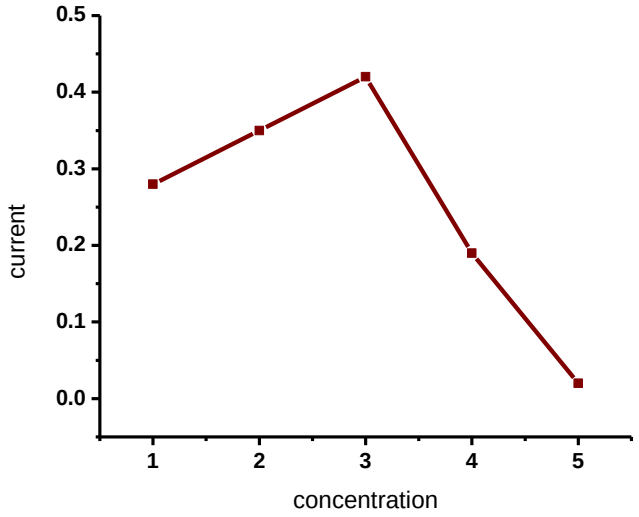

Figure 3.14 *Effect of concentration on short circuit current density*

3.4.3 Concentration effect on open circuit voltage

Open circuit voltage (V_{oc}) is the maximum voltage extracted from a solar cell when current across the circuit is zero. Initially open circuit voltage increases with the increase of dye concentration up to 25μM. By further increasing the dye concentration it starts decreasing due to aggregations of dye molecules on the surface of copper oxide nanoparticles which increases the chances of charge recombination.

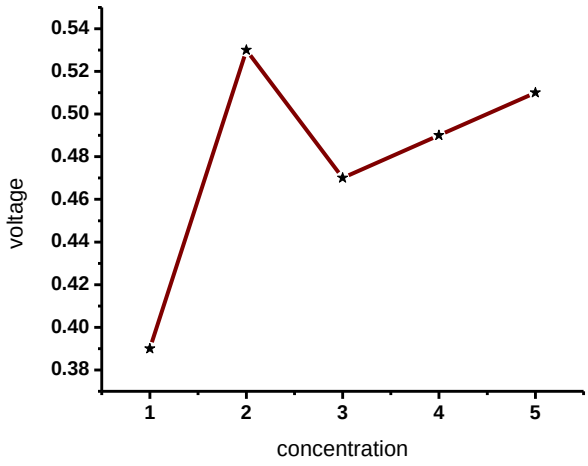

Figure 3.15 *Effect of dye concentration on open circuit voltage*

3.4.4 Fill Factor dependence on dye concentration

The effect of dye concentration on fill factor (FF) is shown in the Fig 3.16. The fill factor gradually decreases with increase of dye concentration and beyond 25μM it starts increasing. By further increasing the dye concentration it again starts decreasing because of charge recombination.

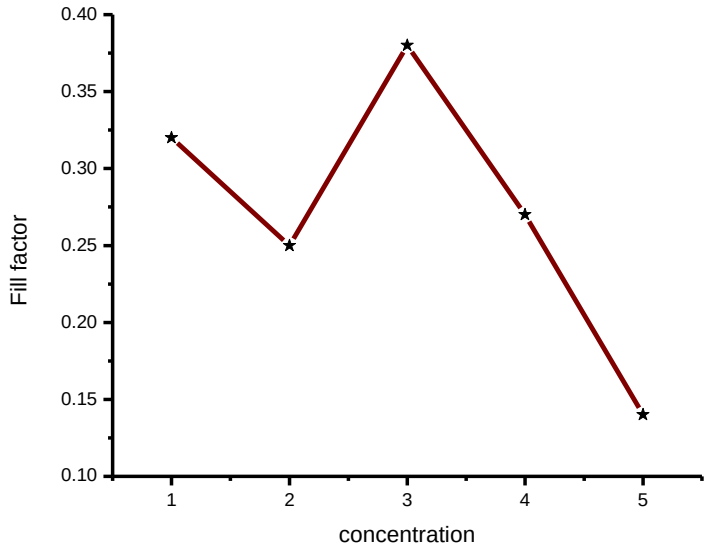

Figure 3.16 *Effect of dye concentration on fill factor*

3.4.5 Effect of dye concentration on maximum power point

Like all other parameters, the concentration of the dye in solar cell also affects the maximum power point values but here the effect on M_{pp} is irregular as shown in the Fig 3.17. Although there is no regular trend of M_{pp} due to concentration, but still it contribute to net efficiency value.

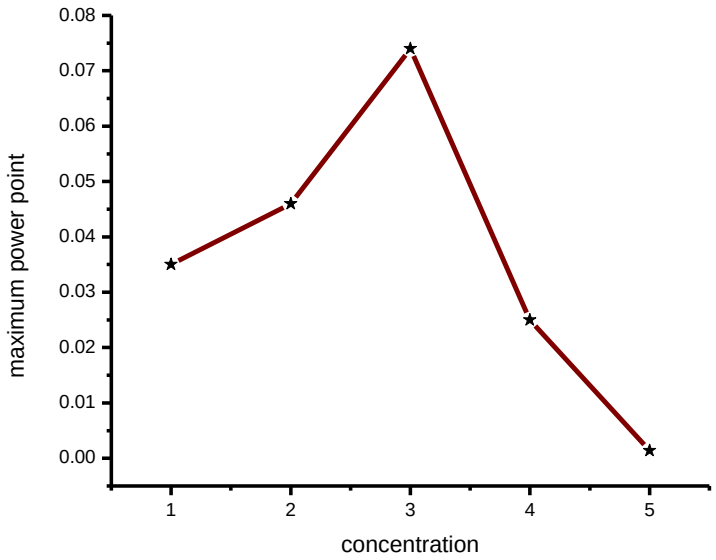

Figure 3.17 *Effect of dye concentration on maximum power point*

CONCLUSION

Copper oxide (CuO) nanoparticles were prepared by sol-gel method with average crystallite size of 13 nm and band gap of 2.13eV. The CuO nanoparticles were successfully functionalized with brilliant blue red (BBR) dye. Solar cells based on functionalized CuO nanoparticles were fabricated by spin-coating method, which showed maximum efficiency of 0.1%. According to the proposed energy level diagram the separated electrons were promoted from the LUMO of the dye to aluminum (Al) electrode while holes were transferred from the HOMO of the dye to valance band of CuO.

REFERENCES

1. Li, Z. and K. Sumathy, *Technology development in the solar absorption air-conditioning systems.* Renewable and sustainable energy reviews, 2000. **4**(3): p. 267-293.
2. Chu, Y., *Review and Comparison of Different Solar Energy Technologies.* Global Energy Network Institute, 2011.
3. Kalkan, N., E. Young, and A. Celiktas, *Solar thermal air conditioning technology reducing the footprint of solar thermal air conditioning.* Renewable and Sustainable Energy Reviews, 2012. **16**(8): p. 6352-6383.
4. Choudhury, B., P. Chatterjee, and J. Sarkar, *Review paper on solar-powered air-conditioning through adsorption route.* Renewable and Sustainable Energy Reviews, 2010. **14**(8): p. 2189-2195.
5. Miles, R.W., G. Zoppi, and I. Forbes, *Inorganic photovoltaic cells.* Materials today, 2007. **10**(11): p. 20-27.
6. Shah, A., et al., *Photovoltaic technology: the case for thin-film solar cells.* science, 1999. **285**(5428): p. 692-698.
7. Williams, R., *Becquerel photovoltaic effect in binary compounds.* The journal of Chemical physics, 1960. **32**(5): p. 1505-1514.
8. Axelrod, N.N., *Volume Photoelectric Effect in Metals.* JOSA, 1966. **56**(2): p. 203-207.
9. Itaya, K., R.E. Malpas, and A.J. Bard, *Photoelectron emission from a metal electrode in liquid ammonia.* Chemical Physics Letters, 1979. **63**(2): p. 411-415.
10. Marion, B., J. del Cueto, and B. Sekulic. *Modeling current–voltage curves using bilinear interpolation*. in *Proceedings of the world renewable energy congress VIII*. 2004.
11. Hegedus, S.S., *Current–Voltage Analysis of a-Si and a-SiGe Solar Cells Including Voltage-dependent Photocurrent Collection.* Progress in Photovoltaics: Research and Applications, 1997. **5**(3): p. 151-168.
12. Chapin, D., C. Fuller, and G. Pearson, *A new silicon p-n junction photocell for converting solar radiation into electrical power.* Journal of Applied Physics, 1954. **25**(5): p. 676-677.
13. Lee, H.-C., et al., *Efficiently harvesting sun light for silicon solar cells through advanced optical couplers and a radial pn junction structure.* Energies, 2010. **3**(4): p. 784-802.
14. Abdellatif, S., et al. *A comparison between Si and GaAs nanowire-based photovoltaic devices*. in *Proc. of SPIE*. 2011.
15. Brown, E. and C. Jigarjian, *Alternative energy: coverage initiated on the solar PV industry*. 2007, Technical report, Bank of America, 162.
16. Camarota, A.G., *Exploring the Elements of Sustainability Management in the Solar Photovoltaic Industry*. 2011, Northcentral University.
17. Shockley, W. and H.J. Queisser, *Detailed balance limit of efficiency of p-n junction solar cells.* Journal of applied physics, 1961. **32**(3): p. 510-519.

18. Tse, P.-K., *China's rare-earth industry*. 2011: US Department of the Interior, US Geological Survey.
19. Bruton, T., *General trends about photovoltaics based on crystalline silicon.* Solar Energy Materials and Solar Cells, 2002. **72**(1): p. 3-10.
20. Dobrzański, L., et al., *Monocrystalline silicon solar cells applied in photovoltaic system.* system, 2012. **53**(1): p. 7-13.
21. Parida, B., S. Iniyan, and R. Goic, *A review of solar photovoltaic technologies.* Renewable and sustainable energy reviews, 2011. **15**(3): p. 1625-1636.
22. Hofstetter, J., et al., *Acceptable contamination levels in solar grade silicon: From feedstock to solar cell.* Materials Science and Engineering: B, 2009. **159**: p. 299-304.
23. Ross, R.T. and T.L. Hsiao, *Limits on the yield of photochemical solar energy conversion.* Journal of Applied Physics, 1977. **48**(11): p. 4783-4785.
24. Shockley, W. and W. Read Jr, *Statistics of the recombinations of holes and electrons.* Physical Review, 1952. **87**(5): p. 835.
25. Hall, R., *Recombination processes in semiconductors.* Proceedings of the IEE-Part B: Electronic and Communication Engineering, 1959. **106**(17S): p. 923-931.
26. Chittick, R., J. Alexander, and H. Sterling, *The preparation and properties of amorphous silicon.* Journal of the Electrochemical Society, 1969. **116**(1): p. 77-81.
27. LeComber, P. and W. Spear, *Doped amorphous semiconductors*, in *Amorphous Semiconductors*. 1985, Springer. p. 251-285.
28. Carlson, D.E. and C.R. Wronski, *Amorphous silicon solar cell.* Applied Physics Letters, 1976. **28**(11): p. 671-673.
29. Kosyachenko, L., *Efficiency of thin-film CdS/CdTe solar cells.* Solar Energy, 2010: p. 105-130.
30. Britt, J. and C. Ferekides, *Thin- film CdS/CdTe solar cell with 15.8% efficiency.* Applied Physics Letters, 1993. **62**(22): p. 2851-2852.
31. O'regan, B. and M. Grfitzeli, *A low-cost, high-efficiency solar cell based on dye-sensitized.* nature, 1991. **353**: p. 737-740.
32. Grätzel, M., *Photoelectrochemical cells.* Nature, 2001. **414**(6861): p. 338-344.
33. Hagfeldt, A. and M. Grätzel, *Molecular photovoltaics.* Accounts of Chemical Research, 2000. **33**(5): p. 269-277.
34. Green, M.A., et al., *Solar cell efficiency tables (version 39).* Progress in photovoltaics: research and applications, 2012. **20**(1): p. 12-20.
35. Chou, T.P., et al., *Titania particle size effect on the overall performance of dye-sensitized solar cells.* The Journal of Physical Chemistry C, 2007. **111**(17): p. 6296-6302.
36. Lee, Y., J. Chae, and M. Kang, *Comparison of the photovoltaic efficiency on DSSC for nanometer sized TiO< sub> 2</sub> using a conventional sol–gel and solvothermal methods.* Journal of Industrial and Engineering Chemistry, 2010. **16**(4): p. 609-614.

37. Wang, Y., *Recent research progress on polymer electrolytes for dye-sensitized solar cells.* Solar Energy Materials and Solar Cells, 2009. **93**(8): p. 1167-1175.
38. Koide, N., et al., *Improvement of efficiency of dye-sensitized solar cells based on analysis of equivalent circuit.* Journal of Photochemistry and Photobiology A: Chemistry, 2006. **182**(3): p. 296-305.
39. Min, J., et al., *Benzimidazole derivatives in the electrolyte of new-generation organic dye-sensitized solar cells with an iodine-free redox mediator.* Journal of Photochemistry and Photobiology A: Chemistry, 2011. **219**(1): p. 148-153.
40. Argazzi, R., et al., *Design of molecular dyes for application in photoelectrochemical and electrochromic devices based on nanocrystalline metal oxide semiconductors.* Coordination Chemistry Reviews, 2004. **248**(13): p. 1299-1316.
41. Kay, A. and M. Grätzel, *Dye-sensitized core-shell nanocrystals: improved efficiency of mesoporous tin oxide electrodes coated with a thin layer of an insulating oxide.* Chemistry of Materials, 2002. **14**(7): p. 2930-2935.
42. Kim, S.-S., J.-H. Yum, and Y.-E. Sung, *Improved performance of a dye-sensitized solar cell using a TiO< sub> 2</sub>/ZnO/Eosin Y electrode.* Solar energy materials and solar cells, 2003. **79**(4): p. 495-505.
43. Kalaignan, G.P. and Y.S. Kang, *A review on mass transport in dye-sensitized nanocrystalline solar cells.* Journal of Photochemistry and Photobiology C: Photochemistry Reviews, 2006. **7**(1): p. 17-22.
44. Ratner, M.A. and D. Ratner, *Nanotechnology: A gentle introduction to the next big idea*. 2003: Prentice Hall Professional.
45. Cahen, D., et al., *Nature of photovoltaic action in dye-sensitized solar cells.* The Journal of Physical Chemistry B, 2000. **104**(9): p. 2053-2059.
46. Huang, S., et al., *Charge recombination in dye-sensitized nanocrystalline TiO2 solar cells.* The Journal of Physical Chemistry B, 1997. **101**(14): p. 2576-2582.
47. Park, N.-G., J. Van de Lagemaat, and A. Frank, *Comparison of dye-sensitized rutile-and anatase-based TiO2 solar cells.* The Journal of Physical Chemistry B, 2000. **104**(38): p. 8989-8994.
48. Zhang, Q., et al., *Aggregation of ZnO Nanocrystallites for High Conversion Efficiency in Dye- Sensitized Solar Cells.* Angewandte Chemie, 2008. **120**(13): p. 2436-2440.
49. Zhang, Q., et al., *Light scattering with oxide nanocrystallite aggregates for dye-sensitized solar cell application.* Journal of Nanophotonics, 2010. **4**(1): p. 041540-041540-23.
50. Nazeeruddin, M.K., et al., *Conversion of light to electricity by cis-X2bis (2, 2'-bipyridyl-4, 4'-dicarboxylate) ruthenium (II) charge-transfer sensitizers (X= Cl-, Br-, I-, CN-, and SCN-) on nanocrystalline titanium dioxide electrodes.* Journal of the American Chemical Society, 1993. **115**(14): p. 6382-6390.

51. Diamant, Y., et al., *Core-shell nanoporous electrode for dye sensitized solar cells: the effect of the SrTiO3 shell on the electronic properties of the TiO2 core.* The Journal of Physical Chemistry B, 2003. **107**(9): p. 1977-1981.
52. Cao, G., *Synthesis, Properties and Applications*. 2004: World Scientific.
53. Chen, X., et al., *Shape-induced ultraviolet absorption of CuO shuttlelike nanoparticles.* Applied physics letters, 2007. **90**(18): p. 183118-183118-3.
54. Allen, R.L.M., *Colour chemistry.* 1971.
55. Kymakis, E., I. Alexandrou, and G. Amaratunga, *High open-circuit voltage photovoltaic devices from carbon-nanotube-polymer composites.* Journal of applied physics, 2003. **93**(3): p. 1764-1768.
56. Taur, Y. and T.H. Ning, *Fundamentals of modern VLSI devices*. Vol. 2. 1998: Cambridge University Press Cambridge.
57. Lanje, A.S., et al., *Synthesis and optical characterization of copper oxide nanoparticles.* Adv Appl Sci Res, 2010. **1**(2): p. 36-40.
58. Wohlfarth, E.P. and K.H.J. Buschow, *Ferromagnetic materials: a handbook on the properties of magnetically ordered substances.* Vol. 2. 1980: Elsevier.
59. Mitsuyu, T., et al., *Piezoelectric thin films of zinc oxide for saw devices.* Ferroelectrics, 1982. **42**(1): p. 233-240.
60. Eliseev, A.A., et al., *Complexes of Cu (II) with polyvinyl alcohol as precursors for the preparation of CuO/SiO2 nanocomposites.* Material Research Innovations, 2000. **3**(5): p. 308-312.
61. Kumar, R.V., Y. Diamant, and A. Gedanken, *Sonochemical synthesis and characterization of nanometer-size transition metal oxides from metal acetates.* Chemistry of Materials, 2000. **12**(8): p. 2301-2305.
62. Son, D.I., C.H. You, and T.W. Kim, *Structural, optical, and electronic properties of colloidal CuO nanoparticles formed by using a colloid-thermal synthesis process.* Applied Surface Science, 2009. **255**(21): p. 8794-8797.
63. Borgohain, K., et al., *Quantum size effects in CuO nanoparticles.* Physical Review B, 2000. **61**(16): p. 11093.
64. Wang, H., et al., *Preparation of CuO nanoparticles by microwave irradiation.* Journal of Crystal Growth, 2002. **244**(1): p. 88-94.
65. Rakhshani, A., *Preparation, characteristics and photovoltaic properties of cuprous oxide—a review.* Solid-State Electronics, 1986. **29**(1): p. 7-17.
66. Mittiga, A., et al., *Heterojunction solar cell with 2% efficiency based on a Cu 2 O substrate.* Applied Physics Letters, 2006. **88**(16): p. 163502-163502-2.
67. Izaki, M., et al., *Electrochemically constructed p-Cu2O/n-ZnO heterojunction diode for photovoltaic device.* Journal of Physics D: Applied Physics, 2007. **40**(11): p. 3326.
68. Oku, T., et al., *Structures and photovoltaic properties of copper oxides/fullerene solar cells.* Journal of Physics and Chemistry of Solids, 2011. **72**(11): p. 1206-1211.

69. Qin, P., et al., *Synthesis and mechanistic studies of organic chromophores with different energy levels for p-type dye-sensitized solar cells.* The Journal of Physical Chemistry C, 2010. **114**(10): p. 4738-4748.
70. Yanagida, S., Y. Yu, and K. Manseki, *Iodine/iodide-free dye-sensitized solar cells.* Accounts of chemical research, 2009. **42**(11): p. 1827-1838.
71. Fan, H., R. Singh, and A. Akbarzadeh, *Electric power generation from thermoelectric cells using a solar dish concentrator*. Journal of electronic materials, 2011. **40**(5): p. 1311-1320.
72. Hart, A.S., et al., *Phenothiazine-sensitized organic solar cells: effect of dye anchor group positioning on the cell performance.* ACS applied materials & interfaces, 2012. **4**(11): p. 5813-5820.
73. Sahay, R., et al., *Synthesis and characterization of CuO nanofibers, and investigation for its suitability as blocking layer in ZnO NPs based dye sensitized solar cell and as photocatalyst in organic dye degradation.* Journal of Solid State Chemistry, 2012. **186**: p. 261-267.
74. Kidowaki, H., et al., *Fabrication and characterization of CuO-based solar cells.* Journal of Materials Science Research, 2012. **1**(1): p. p138.
75. Oku, T., et al., *Microstructures and photovoltaic properties of C60 based solar cells with copper oxides, CuInS2, phthalocyanines, porphyrin, PVK, nanodiamond, germanium and exciton diffusion blocking layers.* Materials Science and Technology, 2013. **28**(1/2): p. 21-39.
76. Raksa, P., et al., *Copper oxide thin film and nanowire as a barrier in ZnO dye-sensitized solar cells.* Thin Solid Films, 2009. **517**(17): p. 4741-4744.
77. KEAT, L.K., *Studies of Cobalt and Iron Oxides/Oxyhydroxides Nanostructures for Electrochemical Applications*. 2013.
78. Aparna, Y., K.E. Rao, and P.S. Subbarao. *Synthesis and characterization of CuO nano particles by novel sol-gel method*. in *Proceedings of the 2nd International Conference on Enviro nment Science and Biotechnology*. 2012.
79. Mustafa, G., et al., *Synthesis and characterization of cupric oxide (CuO) nanoparticles and their application for the removal of dyes.* African Journal of Biotechnology, 2013. **12**(47): p. 6650-6660.